Available online at www.sciencedirect.com
ScienceDirect
Computers & Fluids 36 (2007) 325–341
computers & fluids
www.elsevier.com/locate/compfluid

A continuous adjoint method with objective function derivatives based on boundary integrals, for inviscid and viscous flows

D.I. Papadimitriou, K.C. Giannakoglou *

National Technical University of Athens, School of Mechanical Engineering, Laboratory of Thermal Turbomachines, P.O. Box 64069, 15710 Athens, Greece

Received 14 February 2005; received in revised form 10 November 2005; accepted 28 November 2005
Available online 3 March 2006

Abstract

A continuous adjoint formulation for inverse design problems in external aerodynamics and turbomachinery is presented. The advantage of the proposed formulation is that the objective function gradient does not depend upon the variation of field geometrical quantities, such as metrics variations in the case of structured grids. The final expression for the objective function gradient includes only boundary integrals which can readily be calculated in both structured and unstructured grids; this is feasible in design problems where the objective function is either a boundary integral (pressure deviation along the solid walls) or a field integral (the entropy generation over the flow domain). The formulation governs inviscid and viscous flows; it takes into account the streamtube thickness variation terms in quasi-3D cascade designs or rotational terms in rotating blade design problems. The application of the method is illustrated through a number of design problems concerning isolated airfoils, a 3D duct, 2D, quasi-3D and 3D, stationary and rotating turbomachinery blades.

1. Introduction

Nowadays, a great interest exists upon the development of innovative design and optimization tools for use in aerodynamic shape design and optimization problems. Research focuses on both gradient-based and evolutionary algorithms, with increasing preference to their hybridization. In the first class of methods, the gradient of the objective function with respect to the design variables is required; some recently proposed variants of evolutionary optimization methods [1], may also profit of the availability of objective function gradient values. In the so-called adjoint method, basically inspired by control theory, the gradient can be determined by solving the adjoint equations with coefficients depending on the solution of the flow equations.

Starting from (a) the pde's (Euler or Navier–Stokes equations) which govern a fluid flow problem, (b) an objective function to be minimized and (c) a set of design variables which define the aerodynamic shape of interest, the adjoint method constitutes a tool is capable of computing the objective function gradient. It thus, provides a search direction which can be used in the context of any descent algorithm, in order to minimize the aforesaid objective function. The computation of gradients through the adjoint method has low computational cost compared to the straightforward use of finite-difference schemes; in adjoint methods, the cost for computing the gradient is the same regardless of the number of design variables. The adjoint approach was first introduced by Pironneau [2] for elliptic problems and, then, extended by Jameson [3,4] to transonic flows. In the last decade, the method was further extended to handle supersonic external flows [5,6] as well as steady or unsteady turbomachinery applications [7–10].

Two approaches related to the formulation of the adjoint equations exist; the continuous adjoint method [11–14], in which the adjoint equations are first derived

* Corresponding author. Tel.: +30 210 772 1636; fax: +30 210 772 3789.
E-mail address: kgianna@central.ntua.gr (K.C. Giannakoglou).

0045-7930/$ - see front matter © 2006 Elsevier Ltd. All rights reserved.
doi:10.1016/j.compfluid.2005.11.006

from the flow pde's and then discretized and the discrete one [15,16], in which the discrete adjoint equations are derived from the discretized flow equations. Recently, a series of papers addressing the comparison of the accuracy of these approaches [17,18], have been published. The present paper is dealing exclusively with the continuous adjoint method.

Issues related to the theoretical analysis of the adjoint equations, their boundary conditions or the physical meaning of the adjoint variables are discussed in [19–21]. The major difficulty concerning the use of the adjoint method in real-world design-optimization problems is its inability to handle the so-called inadmissible objective functions; a way to overcome this problem, by introducing of additional adjoint variables and equations, is proposed in [22]. The efficiency of the optimization method can be increased through one-shot algorithms [25], in which the shape is modified and updated in a hierarchical manner. The accuracy of the gradient computed by the adjoint method has been compared with either central difference schemes [23], or the complex variable approach [24].

Another issue is the accurate and inexpensive handling of field grid-coordinate derivatives which appear in the final gradient formula. In the continuous adjoint method, field integrals of $\delta\left(\frac{\partial \Phi}{\partial x_i}\right)$ or $\delta\left(\frac{\partial^2 \Phi}{\partial x_i \partial x_j}\right)$ appear, where Φ is any flow variable; their development gives rise to field integrals involving derivatives of $\delta\Phi$ (readily handled through the Gauss' divergence theorem) as well as derivatives of variations of geometrical quantities. At first glance, the way of handling the latter differ between structured and unstructured grids. For instance, in structured grids, it suffices to proceed with repetitive remeshing after bifurcating one design variable at a time and, then, integrate the metrics variation. This procedure is costly and not applicable to unstructured grids. Motivated by the particular case of mesh variation with fixed geometry, Jameson proposed a development that reduces coordinate sensitivities to the boundary of the flow domain; in [26], this method was used for inviscid design applications. On the other hand, in the discrete adjoint approach, the field terms can be restricted to a near-boundary area, by neglecting the far-field contributions [27].

A different approach is met in [28,29] where the function gradient terms depending on the adjoint variables are not taken into consideration, leading to an incomplete gradient formulation. Although the gradient values differ from those obtained using finite differences, the optimization results are satisfactory and the overall computational cost is comparable to that of the "complete" adjoint approach. A theoretical analysis for the assumptions required for the validity of the proposed method is also found in [28,29].

In the present paper, an adjoint formulation which leads to gradient depending only on the coordinates' variation along the boundaries of the domain is proposed. The herein derived gradient expression is proved to be equivalent to that proposed by Jameson and kim [26], for inviscid flows. Furthermore, it is directly extended to the Navier–Stokes equations, as described below. Extra terms that appear in the equations governing quasi-3D and rotating cascade flows contribute extra boundary integral terms to the gradient. The basic concept is to transform $\delta\left(\frac{\partial \Phi}{\partial x_i}\right)$ or $\delta\left(\frac{\partial^2 \Phi}{\partial x_i \partial x_j}\right)$ to expressions containing gradients of the variations of $\delta\Phi$ and δx_i. The relevant theoretical development is presented in detail. For the sake of completeness, an equivalent development, which assumes structured grids and metrics variations, is presented too. In either case, the resulting formulas are identical and can be applied to both structured and unstructured grids. Any extension to terms including higher order derivatives can be made in a straightforward manner. The Gauss' divergence theorem is then applied to $\delta\Phi$ and δx_i gradients and the field terms depending on coordinate variations are automatically eliminated by imposing and solving the flow and adjoint field equations.

Furthermore, in order to show that the validity of the proposed method is not limited to objective functions expressed as boundary integrals, this was extended to handle also field objective functions. Thus, the adjoint formulation for the minimization of entropy generation in cascades and ducts is also presented. The objective function is transformed into a field integral of temperature and velocity gradients using the boundary layer theory described in [30]. Through the proposed technique, the sensitivity derivatives are expressed only in terms of boundary integrals.

The application of the proposed method on several design-optimization problems for isolated airfoils, duct and cascades is presented. In the reconstruction problems, the target is to capture a known pressure distribution over the solid walls. In the optimization problems, the objective is to minimize the entropy generation through the blade passage which is equivalent to the minimization of total pressure losses. In turbulent flow problems, the Spalart–Allmaras model is used. Depending on the case, structured or unstructured grids are used in order to make clear that the proposed method may handle both of them.

2. Flow equations and objective function

The mathematical formulation of the adjoint method is presented in a form that governs (a) planar flows, (b) quasi-3D flows with streamtube thickness $h(x_1)$ varying along the axial direction x_1 or (c) 3D flows in an either stationary or rotating frame. So, the governing equations for inviscid, laminar or turbulent flows are first written in a unified vector form.

The Navier–Stokes equations may be written as

$$\frac{\partial \mathbf{U}}{\partial t}+\frac{\partial \mathbf{f}_i^{\text{inv}}}{\partial x_i}-\frac{\partial \mathbf{f}_i^{\text{vis}}}{\partial x_i}=\mathbf{Q} \tag{1}$$

where

$$\mathbf{U}=h\begin{bmatrix}\rho\\ \rho\mathbf{V}\\ E\end{bmatrix},\quad \mathbf{f}_i^{\text{inv}}=h\begin{bmatrix}\rho u_i\\ \rho u_i\mathbf{V}+p\delta_i\\ u_i(E+p)\end{bmatrix},\quad \mathbf{f}_i^{\text{vis}}=h\begin{bmatrix}0\\ \tau_i\\ u_j\tau_{ij}+q_i\end{bmatrix} \tag{2}$$

and $\tau_i=[\tau_{i1},\tau_{i2}]^{\mathrm{T}}$ ($\tau_i=[\tau_{i1},\tau_{i2},\tau_{i3}]^{\mathrm{T}}$ in 3D) are the viscous stresses, with

$$\tau_{ij}=\mu\left(\frac{\partial u_i}{\partial x_j}+\frac{\partial u_j}{\partial x_i}\right)+\lambda\delta_{ij}\frac{\partial u_k}{\partial x_k}+\tau^{\star}_{ij},\quad \lambda=-\frac{2}{3}\mu \tag{3}$$

The term $\tau^{\star}_{ij}$ is zero in all but quasi-3D flows, where $\tau^{\star}_{ij}=\mu\delta_{ij}\frac{u_1}{h}\frac{\mathrm{d}h}{\mathrm{d}x_1}$. Also, $\delta_i=[\delta_{i1},\delta_{i2}]^{\mathrm{T}}$ ($\delta_i=[\delta_{i1},\delta_{i2},\delta_{i3}]^{\mathrm{T}}$ in 3D) are the Kronecker symbols, $\mathbf{V}=[u_1,u_2]^{\mathrm{T}}$ ($\mathbf{V}=[u_1,u_2,u_3]^{\mathrm{T}}$ in 3D) is the velocity vector, $q_i=k\frac{\partial T}{\partial x_i}$ and $E=\rho e+\frac{1}{2}\rho u_i^2$. The Einstein convention applies for repeated indices ($i=1,2$ in 2D and $i=1,2,3$ in 3D). The r.h.s. term in Eq. (1) is zero in 2D flows ($\mathbf{Q}=\mathbf{0}$) or given by (quasi-3D flows)

$$\mathbf{Q}=h\frac{\mathrm{d}h}{\mathrm{d}x_1}[0,0,p+\tau_{nn},0]^{\mathrm{T}},\qquad \tau_{nn}=\frac{2}{3}\mu\left(2\frac{u_1}{h}\frac{\mathrm{d}h}{\mathrm{d}x_1}-\frac{\partial u_1}{\partial x_1}-\frac{\partial u_2}{\partial x_2}\right) \tag{4}$$

or (3D flows with constant angular speed ω around the axial direction x_3)

$$\mathbf{Q}=\left[0,-\rho(2\omega u_2+\omega^2 x_1),\rho(2\omega u_1-\omega^2 x_2),0,0\right]^{\mathrm{T}} \tag{5}$$

For the inverse design of aerodynamic shapes which lead to a desired-target pressure distribution $p_{\mathrm{tar}}(S)$ over their solid wall boundaries S_{w}, the objective function is selected to be

$$F=\frac{1}{2}\int_{S_{\mathrm{w}}}(p-p_{\mathrm{tar}})^2\mathrm{d}S \tag{6}$$

By introducing the vector $\boldsymbol{\Psi}$ of the costate variables and computing its inner product with the variation in the flow equations at each point over the flow domain Ω, the variation in the augmented objective function F_{aug} takes the form

$$\delta F_{\mathrm{aug}}=\delta F+\int_{\Omega}\boldsymbol{\Psi}^{\mathrm{T}}\delta\left(\frac{\partial\mathbf{f}_i^{\mathrm{inv}}}{\partial x_i}-\frac{\partial\mathbf{f}_i^{\mathrm{vis}}}{\partial x_i}\right)\mathrm{d}\Omega \tag{7}$$

where

$$\delta F=\frac{1}{2}\int_{S_{\mathrm{w}}}(p-p_{\mathrm{tar}})^2\delta(\mathrm{d}S)+\int_{S_{\mathrm{w}}}(p-p_{\mathrm{tar}})\delta p\,\mathrm{d}S \tag{8}$$

The general formulation of the adjoint equations is totally irrelevant to shape parameterization issues. Note, also, that the objective function for viscous losses minimization problems (field integral of entropy generation) is analyzed in a separate section.

3. A grid-type independent formulation

Any further development of Eq. (7) should be based on the application of the Gauss' divergence theorem. First, terms such as $\delta\left(\frac{\partial\mathbf{f}_i^{\mathrm{inv}}}{\partial x_i}\right)$ or, in general, $\delta\left(\frac{\partial\Phi}{\partial x_i}\right)$, should be cast in divergence form. The transformation proposed below is, in fact, independent of the type of grid used to discretize the flow domain. As it will be proved, it is equivalent to (and inspired from) a recently proposed formulation [27] (restricted however to inviscid flows), which was based on structured grid considerations.

The variation of any flow quantity Φ associated with a (structured or unstructured) grid node, which also varies due to the variation $\delta\mathbf{b}$ in the design variables $\mathbf{b}$, may be written as

$$\delta\Phi=\frac{\partial\Phi}{\partial\mathbf{b}}\delta\mathbf{b}+\frac{\partial\Phi}{\partial x_k}\delta x_k \tag{9}$$

Similarly, the variation of any spatial derivative of Φ, at the same node, reads

$$\delta\left(\frac{\partial\Phi}{\partial x_i}\right)=\frac{\partial}{\partial\mathbf{b}}\left(\frac{\partial\Phi}{\partial x_i}\right)\delta\mathbf{b}+\frac{\partial^2\Phi}{\partial x_i\partial x_k}\delta x_k \tag{10}$$

Furthermore, the derivative of Eq. (9) with respect to x_i can be written as

$$\frac{\partial(\delta\Phi)}{\partial x_i}=\frac{\partial}{\partial x_i}\left(\frac{\partial\Phi}{\partial\mathbf{b}}\right)\delta\mathbf{b}+\frac{\partial^2\Phi}{\partial x_i\partial x_k}\delta x_k+\frac{\partial\Phi}{\partial x_k}\frac{\partial(\delta x_k)}{\partial x_i} \tag{11}$$

so that, by subtracting Eq. (10) from (11), one gets

$$\delta\left(\frac{\partial\Phi}{\partial x_i}\right)=\frac{\partial(\delta\Phi)}{\partial x_i}-\frac{\partial\Phi}{\partial x_k}\frac{\partial(\delta x_k)}{\partial x_i} \tag{12}$$

Eq. (12) is a convenient, general transformation rule that allows the Gauss' divergence theorem to be applied to Eq. (7). Detailed developments, for either inviscid or viscous flows, follow in separate sections.

It is worth commenting more on Eq. (12) and this can be readily done from the viewpoint of a body-fitted coordinate system, typically associated with structured grids. Since the transformed domain in the body-fitted curvilinear coordinates ξ^i space is invariant to $\delta\mathbf{b}$ and, also, $\frac{\partial\Phi}{\partial x_i}=\frac{\partial\Phi}{\partial\xi^j}\frac{\partial\xi^j}{\partial x_i}$, we get

$$\delta\left(\frac{\partial\Phi}{\partial x_i}\right)=\frac{\partial(\delta\Phi)}{\partial x_i}+\frac{\partial\Phi}{\partial\xi^j}\delta\left(\frac{\partial\xi^j}{\partial x_i}\right) \tag{13}$$

Any formulation of the adjoint equations based on Eq. (13) (see also [1,13]) will involve field terms with metrics variations. The use of such a formulation in unstructured grids is, by no means, straightforward. Even in structured grids, the computation of metrics variations increases the CPU cost, especially in complex 3D configurations.

However, according to Appendix A, the metrics variation can be expressed in terms of $\nabla(\delta x_k)$, Eq. (69). Through the latter, Eq. (13) leads again to Eq. (12), which can safely be used regardless of the grid type.

Based on Eq. (12), the integral in Eq. (7) can be written as

$$\int_{\Omega}\boldsymbol{\Psi}^{\mathrm{T}}\delta\left(\frac{\partial\mathbf{f}_i}{\partial x_i}\right)\mathrm{d}\Omega=\int_{\Omega}\boldsymbol{\Psi}^{\mathrm{T}}\frac{\partial(\delta\mathbf{f}_i)}{\partial x_i}\mathrm{d}\Omega-\int_{\Omega}\boldsymbol{\Psi}^{\mathrm{T}}\frac{\partial\mathbf{f}_i}{\partial x_k}\frac{\partial(\delta x_k)}{\partial x_i}\mathrm{d}\Omega \tag{14}$$

where $\mathbf{f}_i$ may stand for either $\mathbf{f}_i^{\mathrm{inv}}$ or $\mathbf{f}_i^{\mathrm{vis}}$. Through integration by parts, Eq. (14) becomes

$$\int_{\Omega}\boldsymbol{\Psi}^{\mathrm{T}}\delta\left(\frac{\partial\mathbf{f}_i}{\partial x_i}\right)\mathrm{d}\Omega=-\int_{\Omega}\delta\mathbf{f}_i^{\mathrm{T}}\frac{\partial\boldsymbol{\Psi}}{\partial x_i}\mathrm{d}\Omega+\int_{S}\boldsymbol{\Psi}^{\mathrm{T}}\delta\mathbf{f}_i n_i\,\mathrm{d}S-\int_{\Omega}\boldsymbol{\Psi}^{\mathrm{T}}\frac{\partial\mathbf{f}_i}{\partial x_k}\frac{\partial(\delta x_k)}{\partial x_i}\mathrm{d}\Omega \tag{15}$$

4. Formulation of the inviscid adjoint equations

The adjoint equations and boundary conditions as well as the final formula for the objective function gradient for inviscid flows are derived. The analysis that follows is valid for 2D or 3D inverse design problems with non-rotating boundaries. Quasi-3D or inverse design problems with rotating components introduce additional terms due to the presence of $\mathbf{Q}$, Eq. (4) or (5), as it will be elaborated in a separate section. In this section, we are dealing only with the Euler equations, $\mathbf{f}_i^{\text{vis}} = \mathbf{0}$, so $\mathbf{f}_i^{\text{inv}}$ will be abbreviated to $\mathbf{f}_i$.

By considering only inviscid fluxes, the first term on the r.h.s. of Eq. (14) is written as

$$\int_\Omega \mathbf{\Psi}^{\mathrm{T}} \frac{\partial(\delta \mathbf{f}_i)}{\partial x_i} \mathrm{d}\Omega = -\int_\Omega \delta \mathbf{U}^{\mathrm{T}} \left(A_i^{\mathrm{T}} \frac{\partial \mathbf{\Psi}}{\partial x_i} \right) \mathrm{d}\Omega + \int_{S_{\mathrm{i,o}}} \mathbf{\Psi}^{\mathrm{T}} \delta \mathbf{f}_i n_i \, \mathrm{d}S + \int_{S_{\mathrm{w}}} \mathbf{\Psi}^{\mathrm{T}} \delta \mathbf{f}_i n_i \, \mathrm{d}S \tag{16}$$

where S_{i}, S_{o}, S_{w} denote the inlet, outlet and solid walls, respectively, $\mathbf{n}$ is the outwards normal vector and $A_i = \frac{\partial \mathbf{f}_i}{\partial \mathbf{U}}$ are the Jacobian matrices. At the inlet or outlet

$$\int_{S_{\mathrm{i,o}}} \mathbf{\Psi}^{\mathrm{T}} \delta \mathbf{f}_i n_i \, \mathrm{d}S = \int_{S_{\mathrm{i,o}}} \delta \mathbf{U}^{\mathrm{T}} (A_n^{\mathrm{T}} \mathbf{\Psi}) \mathrm{d}S \tag{17}$$

where $A_n = A_i n_i$; over the solid wall boundaries, the use of the no-penetration condition $u_i n_i = 0$ gives

$$\int_{S_{\mathrm{w}}} \mathbf{\Psi}^{\mathrm{T}} \delta \mathbf{f}_i n_i \, \mathrm{d}S = \int_{S_{\mathrm{w}}} \Psi_{i+1} n_i \, \delta p \, \mathrm{d}S + \int_{S_{\mathrm{w}}} (\Psi_{i+1} p - \mathbf{\Psi}^{\mathrm{T}} \mathbf{f}_i) \delta(n_i \, \mathrm{d}S) \tag{18}$$

Practically, field terms including $\frac{\partial(\delta x_k)}{\partial x_i}$ (last term on the r.h.s. of Eq. (14)) could be computed on either structured or unstructured grids. A simple way to carry out this computation is through as many remeshing tasks as the number of design variables; thus, it entails extra CPU cost and introduces errors. Alternatively, in this paper it is proposed to integrate this term by parts, so that

$$-\int_\Omega \mathbf{\Psi}^{\mathrm{T}} \frac{\partial \mathbf{f}_i}{\partial x_k} \frac{\partial(\delta x_k)}{\partial x_i} \mathrm{d}\Omega = \int_\Omega \frac{\partial}{\partial x_i} \left(\mathbf{\Psi}^{\mathrm{T}} \frac{\partial \mathbf{f}_i}{\partial x_k} \right) \delta x_k \, \mathrm{d}\Omega - \int_S \mathbf{\Psi}^{\mathrm{T}} \frac{\partial \mathbf{f}_i}{\partial x_k} \delta x_k n_i \, \mathrm{d}S \tag{19}$$

Then, the field integral on the r.h.s. of Eq. (19) can be replaced by

$$\int_\Omega \frac{\partial}{\partial x_i} \left(\mathbf{\Psi}^{\mathrm{T}} \frac{\partial \mathbf{f}_i}{\partial x_k} \right) \delta x_k \, \mathrm{d}\Omega = \int_\Omega \frac{\partial \mathbf{\Psi}^{\mathrm{T}}}{\partial x_i} \frac{\partial \mathbf{f}_i}{\partial x_k} \delta x_k \, \mathrm{d}\Omega + \int_\Omega \mathbf{\Psi}^{\mathrm{T}} \frac{\partial}{\partial x_i} \left(\frac{\partial \mathbf{f}_i}{\partial x_k} \right) \delta x_k \, \mathrm{d}\Omega \tag{20}$$

or

$$\int_\Omega \frac{\partial}{\partial x_i} \left(\mathbf{\Psi}^{\mathrm{T}} \frac{\partial \mathbf{f}_i}{\partial x_k} \right) \delta x_k \, \mathrm{d}\Omega = \int_\Omega \frac{\partial \mathbf{U}^{\mathrm{T}}}{\partial x_k} \left(A_i^{\mathrm{T}} \frac{\partial \mathbf{\Psi}}{\partial x_i} \right) \delta x_k \, \mathrm{d}\Omega + \int_\Omega \mathbf{\Psi}^{\mathrm{T}} \frac{\partial}{\partial x_k} \left(\frac{\partial \mathbf{f}_i}{\partial x_i} \right) \delta x_k \, \mathrm{d}\Omega \tag{21}$$

The last integral on the r.h.s. of Eq. (19), which is meaningful only along the solid walls which are parameterized by the design variables (i.e. where $\delta x_k \neq 0$), is further rewritten as

$$-\int_S \mathbf{\Psi}^{\mathrm{T}} \frac{\partial \mathbf{f}_i}{\partial x_k} \delta x_k n_i \, \mathrm{d}S = -\int_{S_{\mathrm{w}}} \frac{\partial \mathbf{U}^{\mathrm{T}}}{\partial x_k} A_n^{\mathrm{T}} \Psi \delta x_k \, \mathrm{d}S \tag{22}$$

The final expression for the variation in the augmented objective function reads

$$\begin{aligned} \delta F_{\mathrm{aug}} = {} & \underbrace{\frac{1}{2} \int_{S_{\mathrm{w}}} (p - p_{\mathrm{tar}})^2 \delta(\mathrm{d}S)}_{B.S.D.} + \underbrace{\int_{S_{\mathrm{w}}} (p - p_{\mathrm{tar}}) \delta p \, \mathrm{d}S}_{B.C.1} \\ & \underbrace{- \int_\Omega \left(\delta \mathbf{U}^{\mathrm{T}} - \frac{\partial \mathbf{U}^{\mathrm{T}}}{\partial x_k} \delta x_k \right) \left(A_i^{\mathrm{T}} \frac{\partial \mathbf{\Psi}}{\partial x_i} \right) \mathrm{d}\Omega}_{F.A.E.} \\ & + \underbrace{\int_\Omega \mathbf{\Psi}^{\mathrm{T}} \frac{\partial}{\partial x_k} \left(\frac{\partial \mathbf{f}_i}{\partial x_i} \right) \delta x_k \, \mathrm{d}\Omega}_{D.F.E.} - \underbrace{\int_{S_{\mathrm{w}}} \frac{\partial \mathbf{U}^{\mathrm{T}}}{\partial x_k} A_n^{\mathrm{T}} \mathbf{\Psi} \, \delta x_k \, \mathrm{d}S}_{B.S.D.} \\ & + \underbrace{\int_{S_{\mathrm{w}}} \Psi_{i+1} n_i \, \delta p \, \mathrm{d}S}_{B.C.2} + \underbrace{\int_{S_{\mathrm{w}}} (\Psi_{i+1} p - \mathbf{\Psi}^{\mathrm{T}} \mathbf{f}_i) \delta(n_i \, \mathrm{d}S)}_{B.S.D.} \\ & + \underbrace{\int_{S_{\mathrm{i,o}}} \delta \mathbf{U}^{\mathrm{T}} (A_n^{\mathrm{T}} \mathbf{\Psi}) \mathrm{d}S}_{B.C.3} \end{aligned} \tag{23}$$

where the term marked with *D.F.E.* is, evidently, zero. By choosing $\mathbf{\Psi}$ to satisfy the field adjoint equations

$$\frac{\partial \mathbf{\Psi}}{\partial t} - A_i^{\mathrm{T}} \frac{\partial \mathbf{\Psi}}{\partial x_i} = \mathbf{0} \tag{24}$$

with inlet–outlet boundary conditions determined by

$$\delta \mathbf{U}^{\mathrm{T}} (A_n^{\mathrm{T}} \mathbf{\Psi}) = \mathbf{0} \tag{25}$$

terms marked with (*F.A.E.*) and (*B.C.*3) in Eq. (23) are eliminated. Terms denoted by *B.C.*1 and *B.C.*2 are also eliminated by imposing

$$(p - p_{\mathrm{tar}}) + \Psi_{i+1} n_i = 0 \tag{26}$$

over S_{w}. The remaining terms in Eq. (23), marked with (*B.S.D.*), express the objective function derivatives with respect to the design variables, namely

$$\delta F_{\mathrm{aug}} = \frac{1}{2} \int_{S_{\mathrm{w}}} (p - p_{\mathrm{tar}})^2 \delta(\mathrm{d}S) - \int_{S_{\mathrm{w}}} \frac{\partial \mathbf{U}^{\mathrm{T}}}{\partial x_k} A_n^{\mathrm{T}} \mathbf{\Psi} \delta x_k \, \mathrm{d}S + \int_{S_{\mathrm{w}}} (\Psi_{i+1} p - \mathbf{\Psi}^{\mathrm{T}} \mathbf{f}_i) \delta(n_i \, \mathrm{d}S) \tag{27}$$

Eq. (27) could further be worked out only after defining the shape parameterization.

For the sake of comparison, the variation in F_{aug} expressed in terms of metrics variations (using Eq. (13) instead of Eq. (12)) is also provided; it reads

$$\delta F_{\text{aug}} = \underbrace{\frac{1}{2}\int_{S_w}(p-p_{\text{tar}})^2\delta(\mathrm{d}S)}_{B.S.D.} + \underbrace{\int_{S_w}(p-p_{\text{tar}})\delta p\,\mathrm{d}S}_{B.C.1} - \underbrace{\int_\Omega \delta\mathbf{U}^{\mathrm{T}}\left(A_i^{\mathrm{T}}\frac{\partial\boldsymbol{\Psi}}{\partial x_i}\right)\mathrm{d}\Omega}_{F.A.E.} + \underbrace{\int_\Omega \boldsymbol{\Psi}^{\mathrm{T}}\frac{\partial f_i}{\partial\xi^j}\delta\left(\frac{\partial\xi^j}{\partial x_i}\right)\mathrm{d}\Omega}_{F.S.D.} + \underbrace{\int_{S_w}\Psi_{i+1}n_i\,\delta p\,\mathrm{d}S}_{B.C.2} + \underbrace{\int_{S_w}(\Psi_{i+1}p-\boldsymbol{\Psi}^{\mathrm{T}}\mathbf{f}_i)\delta(n_i\,\mathrm{d}S)}_{B.S.D.} + \underbrace{\int_{S_{i,o}}\delta\mathbf{U}^{\mathrm{T}}(A_n^{\mathrm{T}}\boldsymbol{\Psi})\mathrm{d}S}_{B.C.3} \tag{28}$$

and is practically valid only for structured grids. The field and boundary adjoint equations are the same analyzed above but the gradient of the objective function is given by the expression

$$\delta F_{\text{aug}} = \frac{1}{2}\int_{S_w}(p-p_{\text{tar}})^2\delta(\mathrm{d}S) - \int_\Omega \boldsymbol{\Psi}^{\mathrm{T}}\frac{\partial f_i}{\partial\xi^j}\delta\left(\frac{\partial\xi^j}{\partial x_i}\right)\mathrm{d}\Omega + \int_{S_w}(\Psi_{i+1}p-\boldsymbol{\Psi}^{\mathrm{T}}\mathbf{f}_i)\delta(n_i\,\mathrm{d}S) \tag{29}$$

instead of Eq. (27). At each optimization cycle, the computation of the second term on the r.h.s. requires as many calls to the grid generator as the number of design variables.

5. Formulation of the viscous adjoint equations

The objective of this section is to present a similar approach for the development of the adjoint equations for (laminar or turbulent) viscous flow problems. Two assumptions are made: the viscosity coefficients are assumed to be independent of temperature and, for turbulent flows, the turbulent viscosity variation is left out [13].

Now, $\mathbf{f}_i^{\text{vis}}$ is abbreviated to $\mathbf{f}_i$. Eqs. (14) and (15) are still the keypoint for the mathematical development of the viscous terms in Eq. (7). Using the expression for the viscous fluxes, the first field term on the r.h.s. of Eq. (15) reads

$$\int_\Omega \delta\mathbf{f}_i^{\mathrm{T}}\frac{\partial\boldsymbol{\Psi}}{\partial x_i}\mathrm{d}\Omega = \int_\Omega\left[\delta\tau_{ij}\left(\frac{\partial\Psi_{j+1}}{\partial x_i}+u_j\frac{\partial\Psi_m}{\partial x_i}\right) + \delta u_j\left(\tau_{ij}\frac{\partial\Psi_m}{\partial x_i}\right)+\delta q_i\frac{\partial\Psi_m}{\partial x_i}\right]\mathrm{d}\Omega \tag{30}$$

where $m=4$ in 2D or $m=5$ in 3D problems. According to Eq. (3), the variation in stresses $\delta\tau_{ij}$ can be expressed in terms of variations in the velocity components and geo- metry, as follows:

$$\delta\tau_{ij} = \mu\left[\frac{\partial(\delta u_i)}{\partial x_j}+\frac{\partial(\delta u_j)}{\partial x_i}\right]+\lambda\delta_{ij}\frac{\partial(\delta u_k)}{\partial x_k} - \mu\left[\frac{\partial u_i}{\partial x_k}\frac{\partial(\delta x_k)}{\partial x_j}+\frac{\partial u_j}{\partial x_k}\frac{\partial(\delta x_k)}{\partial x_i}\right]-\lambda\delta_{ij}\frac{\partial u_l}{\partial x_k}\frac{\partial(\delta x_k)}{\partial x_l} \tag{31}$$

Then, the first term on the r.h.s. of Eq. (30) reads

$$\begin{aligned}\int_\Omega \delta\tau_{ij}\left(\frac{\partial\Psi_{j+1}}{\partial x_i}+u_j\frac{\partial\Psi_m}{\partial x_i}\right)\mathrm{d}\Omega &= \int_\Omega\left\{\mu\left[\frac{\partial(\delta u_i)}{\partial x_j}+\frac{\partial(\delta u_j)}{\partial x_i}\right]+\lambda\delta_{ij}\frac{\partial(\delta u_k)}{\partial x_k}\right\}\times\left(\frac{\partial\Psi_{j+1}}{\partial x_i}+u_j\frac{\partial\Psi_m}{\partial x_i}\right)\mathrm{d}\Omega\\ &-\int_\Omega\left\{\mu\left[\frac{\partial u_i}{\partial x_k}\frac{\partial(\delta x_k)}{\partial x_j}+\frac{\partial u_j}{\partial x_k}\frac{\partial(\delta x_k)}{\partial x_i}\right]+\lambda\delta_{ij}\frac{\partial u_l}{\partial x_k}\frac{\partial(\delta x_k)}{\partial x_l}\right\}\times\left(\frac{\partial\Psi_{j+1}}{\partial x_i}+u_j\frac{\partial\Psi_m}{\partial x_i}\right)\mathrm{d}\Omega\end{aligned} \tag{32}$$

Through integration by parts and after the rearrangement of indices, the first field integral on the right may be written as

$$\begin{aligned}&\int_\Omega\left\{\mu\left[\frac{\partial(\delta u_i)}{\partial x_j}+s\frac{\partial(\delta u_j)}{\partial x_i}\right]+\lambda\delta_{ij}\frac{\partial(\delta u_k)}{\partial x_k}\right\}\left(\frac{\partial\Psi_{j+1}}{\partial x_i}+u_j\frac{\partial\Psi_m}{\partial x_i}\right)\mathrm{d}\Omega\\ &=-\int_\Omega\delta u_i\frac{\partial}{\partial x_j}\left[\mu\left(\frac{\partial\Psi_{j+1}}{\partial x_i}+u_j\frac{\partial\Psi_m}{\partial x_i}+\frac{\partial\Psi_{i+1}}{\partial x_j}+u_i\frac{\partial\Psi_m}{\partial x_j}\right)+\lambda\delta_{ij}\left(\frac{\partial\Psi_{k+1}}{\partial x_k}+u_k\frac{\partial\Psi_m}{\partial x_k}\right)\right]\mathrm{d}\Omega+\int_S\delta u_i\left[\mu\left(\frac{\partial\Psi_{j+1}}{\partial x_i}+u_j\frac{\partial\Psi_m}{\partial x_i}\right.\right.\\ &\left.\left.+\frac{\partial\Psi_{i+1}}{\partial x_j}+u_i\frac{\partial\Psi_m}{\partial x_j}\right)+\lambda\delta_{ij}\left(\frac{\partial\Psi_{k+1}}{\partial x_k}+u_k\frac{\partial\Psi_m}{\partial x_k}\right)\right]n_j\mathrm{d}S\end{aligned} \tag{33}$$

The integration by parts of the second term on the r.h.s. of Eq. (32), gives

$$\begin{aligned}&-\int_\Omega\left\{\mu\left[\frac{\partial u_i}{\partial x_k}\frac{\partial(\delta x_k)}{\partial x_j}+\frac{\partial u_j}{\partial x_k}\frac{\partial(\delta x_k)}{\partial x_i}\right]+\lambda\delta_{ij}\frac{\partial u_l}{\partial x_k}\frac{\partial(\delta x_k)}{\partial x_l}\right\}\times\left(\frac{\partial\Psi_{j+1}}{\partial x_i}+u_j\frac{\partial\Psi_m}{\partial x_i}\right)\mathrm{d}\Omega=\int_\Omega\frac{\partial\tau_{ij}}{\partial x_l}\left(\frac{\partial\Psi_{j+1}}{\partial x_i}+u_j\frac{\partial\Psi_m}{\partial x_i}\right)\delta x_l\,\mathrm{d}\Omega\\ &+\int_\Omega\frac{\partial u_i}{\partial x_l}\frac{\partial}{\partial x_j}\left[\mu\left(\frac{\partial\Psi_{j+1}}{\partial x_i}+u_j\frac{\partial\Psi_m}{\partial x_i}+\frac{\partial\Psi_{i+1}}{\partial x_j}+u_i\frac{\partial\Psi_m}{\partial x_j}\right)+\lambda\delta_{ij}\left(\frac{\partial\Psi_{k+1}}{\partial x_k}+u_k\frac{\partial\Psi_m}{\partial x_k}\right)\right]\delta x_l\,\mathrm{d}\Omega\\ &-\int_S\frac{\partial u_i}{\partial x_l}\left[\mu\left(\frac{\partial\Psi_{j+1}}{\partial x_i}+u_j\frac{\partial\Psi_m}{\partial x_i}+\frac{\partial\Psi_{i+1}}{\partial x_j}+u_i\frac{\partial\Psi_m}{\partial x_j}\right)+\lambda\delta_{ij}\left(\frac{\partial\Psi_{k+1}}{\partial x_k}+u_k\frac{\partial\Psi_m}{\partial x_k}\right)\right]\delta x_l n_j\mathrm{d}S\end{aligned} \tag{34}$$

The term which depends on the thermal flux variation, Eq. (30), is written as

$$\int_\Omega\delta q_i\frac{\partial\Psi_m}{\partial x_i}\mathrm{d}\Omega=\int_\Omega k\left[\frac{\partial(\delta T)}{\partial x_i}-\frac{\partial T}{\partial x_k}\frac{\partial(\delta x_k)}{\partial x_i}\right]\frac{\partial\Psi_m}{\partial x_i}\mathrm{d}\Omega \tag{35}$$

The first term on the r.h.s. of Eq. (35) is integrated by parts to give

$$\int_\Omega k\frac{\partial(\delta T)}{\partial x_i}\frac{\partial\Psi_m}{\partial x_i}\mathrm{d}\Omega=-\int_\Omega\delta T\frac{\partial}{\partial x_i}\left(k\frac{\partial\Psi_m}{\partial x_i}\right)\mathrm{d}\Omega+\int_S\delta T\left(k\frac{\partial\Psi_m}{\partial x_i}n_i\right)\mathrm{d}S \tag{36}$$

The second term in the r.h.s. integral of Eq. (35) is also integrated by parts and yields

$$-\int_\Omega k\frac{\partial T}{\partial x_k}\frac{\partial(\delta x_k)}{\partial x_i}\frac{\partial \Psi_m}{\partial x_i}\mathrm{d}\Omega=\int_\Omega \frac{\partial q_i}{\partial x_k}\frac{\partial \Psi_m}{\partial x_i}\delta x_k\,\mathrm{d}\Omega+\int_\Omega \frac{\partial T}{\partial x_k}\frac{\partial}{\partial x_i}\left(k\frac{\partial \Psi_m}{\partial x_i}\right)\delta x_k\,\mathrm{d}\Omega-\int_S k\frac{\partial T}{\partial x_k}\frac{\partial \Psi_m}{\partial x_i}\delta x_k n_i\,\mathrm{d}S \quad (37)$$

The surface integral in Eq. (15) is further analyzed as follows:

$$-\int_S \mathbf{\Psi}^{\mathrm{T}}\delta\mathbf{f}_i n_i\,\mathrm{d}S=-\int_S[(\Psi_{i+1}+u_i\Psi_m)\delta\tau_{ij}+\Psi_m\tau_{ij}\delta u_i+\Psi_m\delta q_j]n_j\,\mathrm{d}S \quad (38)$$

In viscous flows, the relation $\frac{\partial V_n}{\partial n}=0$ over the solid wall nodes leads to $\tau_{ij}n_in_j=0$ or, equivalently,

$$\delta\tau_{ij}n_in_j+\tau_{ij}\delta(n_in_j)=0 \quad (39)$$

So, the first term on the r.h.s. of Eq. (38) is rewritten as

$$-\int_S \Psi_{i+1}\delta\tau_{ij}n_j\,\mathrm{d}S=-\int_S\frac{\Psi_{i+1}}{n_i}[\delta\tau_{ij}n_in_j+\tau_{ij}\delta(n_in_j)]\mathrm{d}S+\int_S\frac{\Psi_{i+1}}{n_i}\tau_{ij}\delta(n_in_j)\mathrm{d}S \quad (40)$$

The last term in Eq. (15) is integrated by parts to give

$$\int_\Omega \mathbf{\Psi}^{\mathrm{T}}\frac{\partial\mathbf{f}_i}{\partial x_k}\frac{\partial(\delta x_k)}{\partial x_i}\mathrm{d}\Omega=-\int_\Omega\left(\frac{\partial\mathbf{f}_i}{\partial x_k}\right)^{\mathrm{T}}\frac{\partial\mathbf{\Psi}}{\partial x_i}\delta x_k\,\mathrm{d}\Omega-\int_\Omega\mathbf{\Psi}^{\mathrm{T}}\frac{\partial}{\partial x_k}\left(\frac{\partial\mathbf{f}_i}{\partial x_i}\right)\delta x_k\,\mathrm{d}\Omega+\int_S\left(\mathbf{\Psi}^{\mathrm{T}}\frac{\partial\mathbf{f}_i}{\partial x_k}\right)\delta x_k n_i\,\mathrm{d}S \quad (41)$$

From the equation of state, $\delta T=-\frac{T}{\rho}\delta\rho+\frac{T}{p}\delta p$. Finally, it is convenient to define $\mathbf{K}=(K_1,\ldots,K_m)^{\mathrm{T}}$ as follows

$$\begin{aligned}K_1&=-\frac{T}{\rho}\frac{\partial}{\partial x_i}\left(k\frac{\partial\Psi_m}{\partial x_i}\right)\\K_{i+1}&=\frac{\partial}{\partial x_j}\left[\mu\left(\frac{\partial\Psi_{j+1}}{\partial x_i}+u_j\frac{\partial\Psi_m}{\partial x_i}+\frac{\partial\Psi_{i+1}}{\partial x_j}+u_i\frac{\partial\Psi_m}{\partial x_j}\right)+\lambda\delta_{ij}\left(\frac{\partial\Psi_{k+1}}{\partial x_k}+u_k\frac{\partial\Psi_m}{\partial x_k}\right)\right]-\tau_{ij}\frac{\partial\Psi_m}{\partial x_j}\\K_m&=\frac{T}{p}\frac{\partial}{\partial x_i}\left(k\frac{\partial\Psi_m}{\partial x_i}\right)\end{aligned} \quad (42)$$

so, with the help of previous expressions, the variation in F_{aug} is

$$\begin{aligned}\delta F_{\mathrm{aug}}=&\underbrace{\frac{1}{2}\int_{S_w}(p-p_{\mathrm{tar}})^2\delta(\mathrm{d}S)}_{B.S.D.}+\underbrace{\int_{S_w}(p-p_{\mathrm{tar}})\delta p\mathrm{d}S}_{B.C.1}-\underbrace{\int_\Omega\left(\delta\mathbf{U}-\frac{\partial\mathbf{U}}{\partial x_k}\delta x_k\right)^{\mathrm{T}}\left(A_i^{\mathrm{T}}\frac{\partial\mathbf{\Psi}}{\partial x_i}\right)\mathrm{d}\Omega}_{F.A.E.}\\&-\underbrace{\int_\Omega\left(\delta\mathbf{W}-\frac{\partial\mathbf{W}}{\partial x_k}\delta x_k\right)^{\mathrm{T}}\mathbf{K}\mathrm{d}\Omega}_{F.A.E.}+\underbrace{\int_\Omega\mathbf{\Psi}^{\mathrm{T}}\frac{\partial}{\partial x_k}\left(\frac{\partial\mathbf{f}_i^{\mathrm{inv}}}{\partial x_i}-\frac{\partial\mathbf{f}_i^{\mathrm{vis}}}{\partial x_i}\right)\delta x_k\,\mathrm{d}\Omega}_{D.F.E.}\\&-\underbrace{\int_{S_w}\frac{\partial\mathbf{U}^{\mathrm{T}}}{\partial x_k}(A_i^{\mathrm{T}}n_i)\mathbf{\Psi}\delta x_k\,\mathrm{d}S}_{B.S.D.}+\underbrace{\int_{S_w}\Psi_i n_i\delta p\mathrm{d}S}_{B.C.2}+\underbrace{\int_{S_w}(\Psi_i p-\mathbf{\Psi}^{\mathrm{T}}\mathbf{f}_i)\delta(n_i\mathrm{d}S)}_{B.S.D.}+\underbrace{\int_{S_{i,o}}\delta\mathbf{U}^{\mathrm{T}}(A_n^{\mathrm{T}}\mathbf{\Psi})\mathrm{d}S}_{B.C.3}\\&+\underbrace{\int_{S_w}\delta u_i\left[\mu\left(\frac{\partial\Psi_{j+1}}{\partial x_i}+u_j\frac{\partial\Psi_m}{\partial x_i}+\frac{\partial\Psi_{i+1}}{\partial x_j}+u_i\frac{\partial\Psi_m}{\partial x_j}\right)+\lambda\delta_{ij}\left(\frac{\partial\Psi_{k+1}}{\partial x_k}+u_k\frac{\partial\Psi_m}{\partial x_k}\right)-\Psi_m\tau_{ij}\right]n_j\mathrm{d}S}_{B.C.4}\\&+\underbrace{\int_{S_w}\delta T\left(k\frac{\partial\Psi_m}{\partial x_i}n_i\right)\mathrm{d}S}_{B.C.5}-\underbrace{\int_{S_w}\Psi_m\delta(q_jn_j\mathrm{d}S)}_{B.C.6}+\underbrace{\int_{S_w}\Psi_mq_j\delta(n_j\mathrm{d}S)}_{B.S.D.}\\&-\underbrace{\int_{S_w}\frac{\Psi_{i+1}}{n_i}[\delta\tau_{ij}n_in_j+\tau_{ij}\delta(n_in_j)]\mathrm{d}S}_{B.C.7}+\underbrace{\int_{S_w}\frac{\Psi_{i+1}}{n_i}\tau_{ij}\delta(n_in_j)\mathrm{d}S}_{B.S.D.}-\underbrace{\int_{S_w}u_i\Psi_m\delta\tau_{ij}n_j\,\mathrm{d}S}_{B.C.8}\\&-\underbrace{\int_{S_w}\frac{\partial u_i}{\partial x_l}\left[\mu\left(\frac{\partial\Psi_{j+1}}{\partial x_i}+u_j\frac{\partial\Psi_m}{\partial x_i}+\frac{\partial\Psi_{i+1}}{\partial x_j}+u_i\frac{\partial\Psi_m}{\partial x_j}\right)+\lambda\delta_{ij}\left(\frac{\partial\Psi_{k+1}}{\partial x_k}+u_k\frac{\partial\Psi_m}{\partial x_k}\right)\right]\delta x_ln_j\mathrm{d}S}_{B.S.D.}\\&+\underbrace{\int_{S_w}\frac{\partial T}{\partial x_k}\left(k\frac{\partial\Psi_m}{\partial x_i}\right)\delta x_kn_i\,\mathrm{d}S}_{B.S.D}-\underbrace{\int_{S_w}\left(\mathbf{\Psi}^{\mathrm{T}}\frac{\partial\mathbf{f}_i^{\mathrm{vis}}}{\partial x_k}\right)\delta x_kn_i\mathrm{d}S}_{B.S.D.}\end{aligned} \quad (43)$$

where $\mathbf{W}=[\rho,\mathbf{V},p]^{\mathrm{T}}$ is the vector of non-conservative variables. It should be noted that integrals marked with *B.C.*4 to *B.C.*8 should be computed over the solid walls S_{w} (instead of S), since the derivatives of flow or adjoint variables at the inlet and exit can safely be neglected.

Using the transformation matrix from non-conservative to conservative variables, $M=\frac{\partial U}{\partial W}$, the terms marked with *F.A.E.* can be eliminated by satisfying the field adjoint equations

$$\frac{\partial\mathbf{\Psi}}{\partial t}-A_i^{\mathrm{T}}\frac{\partial\mathbf{\Psi}}{\partial x_i}-M^{-T}\mathbf{K}=\mathbf{0} \quad (44)$$

which is the extension of Eq. (24) for viscous flows. Likely to inviscid flow problems, the inlet and outlet boundary conditions are derived from the term marked with *B.C.*3. Regarding inlet and outlet, terms marked with *B.C.*4–*B.C.*8 may or may not be taken into consideration since, there, the flow and adjoint variable derivatives and their variations are negligible.

With the help of Eq. (39), term *B.C.*7 is eliminated provided that $\frac{\Psi_{i+1}}{n_i}$ is the same for all $i=1,2(3)$ (no summation). This condition, together with Eq. (26) that comes from *B.C.*1 and *B.C.*2, defines the condition for the velocity adjoint variables (Ψ_2, Ψ_3 in 2D or Ψ_2, Ψ_3, Ψ_4 in 3D) over S_{w}, namely

$$\Psi_{i+1}=-(p-p_{\mathrm{tar}})n_i,\quad i=1,2(3) \quad (45)$$

Terms marked with *B.C.*4 and *B.C.*8 are equal to zero since velocities and their variations are all zero over S_{w}. The elimination of terms *B.C.*5 and *B.C.*6 determines the boundary condition for Ψ_m over S_{w}. It should be noted that Ψ_m depends on the type of temperature conditions along the solid walls. For constant wall temperature, *B.C.*5 is zero and *B.C.*6 determines zero Dirichlet condition for Ψ_m ($\Psi_m=0$). In contrast, for adiabatic flow conditions, *B.C.*6 is zero and *B.C.*5 leads to zero Neumann condition for Ψ_m ($\frac{\partial\Psi_m}{\partial n}=0$).

The remaining terms in Eq. (43), which are all marked with *B.S.D.*, depend on variations in geometrical quantities and, thus, on variations in the design variables. Finally, Eq. (43) can be written as

$$\begin{aligned}\delta F_{\mathrm{aug}}=&\frac{1}{2}\int_{S_w}(p-p_{\mathrm{tar}})^2\delta(\mathrm{d}S)+\int_{S_w}(\Psi_ip-\mathbf{\Psi}^{\mathrm{T}}\mathbf{f}_i)\delta(n_i\,\mathrm{d}S)\\&-\int_{S_w}\frac{\partial\mathbf{U}^{\mathrm{T}}}{\partial x_k}(A_i^{\mathrm{T}}n_i)\mathbf{\Psi}\,\delta x_k\,\mathrm{d}S+\int_{S_w}\left(\mathbf{\Psi}^{\mathrm{T}}\frac{\partial\mathbf{f}_{vi}}{\partial x_k}\right)\delta x_kn_i\,\mathrm{d}S\\&+\int_{S_w}\frac{\Psi_{i+1}}{n_i}\tau_{ij}\delta(n_in_j)\,\mathrm{d}S+\int_{S_w}\Psi_mq_j\delta(n_j\,\mathrm{d}S)\end{aligned}$$

$$-\int_{S_w}\frac{\partial u_i}{\partial x_l}\left[\mu\left(\frac{\partial \Psi_{j+1}}{\partial x_i}+u_j\frac{\partial \Psi_m}{\partial x_i}+\frac{\partial \Psi_{i+1}}{\partial x_j}+u_i\frac{\partial \Psi_m}{\partial x_j}\right)+\lambda\delta_{ij}\left(\frac{\partial \Psi_{k+1}}{\partial x_k}+u_k\frac{\partial \Psi_m}{\partial x_k}\right)\right]\delta x_l n_j\,\mathrm{d}S \quad (46)$$

In the case of using Eq. (13) instead of Eq. (12), the Gauss' divergence theorem is applied twice for the terms depending on the gradient of flow variables' variations. The variation in F_{aug} now reads

$$\begin{aligned}\delta F_{\mathrm{aug}} =& \underbrace{\frac{1}{2}\int_{S_w}(p-p_{\mathrm{tar}})^2\delta(\mathrm{d}S)}_{B.S.D.}+\underbrace{\int_{S_w}(p-p_{\mathrm{tar}})\delta p\,\mathrm{d}S}_{B.C.1}\\ &-\underbrace{\int_\Omega \delta\mathbf{U}^{\mathrm{T}}\left(A_i^{\mathrm{T}}\frac{\partial \boldsymbol{\Psi}}{\partial x_i}\right)\mathrm{d}\Omega}_{F.A.E.}-\underbrace{\int_\Omega \delta\mathbf{W}^{\mathrm{T}}\mathbf{K}\mathrm{d}\Omega}_{F.A.E.}\\ &+\underbrace{\int_{S_w}\Psi_i n_i\delta p\,\mathrm{d}S}_{B.C.2}+\underbrace{\int_{S_w}(\Psi_i p-\boldsymbol{\Psi}^{\mathrm{T}}\mathbf{f}_i)\delta(n_i\,\mathrm{d}S)}_{B.S.D.}+\underbrace{\int_{S_{i,o}}\delta\mathbf{U}^{\mathrm{T}}(A_n^{\mathrm{T}}\boldsymbol{\Psi})\mathrm{d}S}_{B.C.3}\\ &+\underbrace{\int_{S_w}\delta u_i\left[\mu\left(\frac{\partial \Psi_{j+1}}{\partial x_i}+u_j\frac{\partial \Psi_m}{\partial x_i}+\frac{\partial \Psi_{i+1}}{\partial x_j}+u_i\frac{\partial \Psi_m}{\partial x_j}\right)+\lambda\delta_{ij}\left(\frac{\partial \Psi_{k+1}}{\partial x_k}+u_k\frac{\partial \Psi_m}{\partial x_k}\right)-\Psi_m\tau_{ij}\right]n_j\,\mathrm{d}S}_{B.C.4}\\ &+\underbrace{\int_{S_w}\delta T\left(k\frac{\partial \Psi_m}{\partial x_i}n_i\right)\mathrm{d}S}_{B.C.5}-\underbrace{\int_{S_w}\Psi_m\delta(q_j n_j\mathrm{d}S)}_{B.C.6}+\underbrace{\int_{S_w}\Psi_m q_j\delta(n_j\,\mathrm{d}S)}_{B.S.D.}\\ &-\underbrace{\int_{S_w}\frac{\Psi_{i+1}}{n_i}[\delta\tau_{ij}n_i n_j+\tau_{ij}\delta(n_i n_j)]\mathrm{d}S}_{B.C.7}+\underbrace{\int_{S_w}\frac{\Psi_{i+1}}{n_i}\tau_{ij}\delta(n_i n_j)\mathrm{d}S}_{B.S.D.}-\underbrace{\int_{S_w}u_i\Psi_m\delta\tau_{ij}n_j\,\mathrm{d}S}_{B.C.8}\\ &+\underbrace{\int_\Omega\boldsymbol{\Psi}^{\mathrm{T}}\left(\frac{\partial f_i^{\mathrm{inv}}}{\partial\xi^j}-\frac{\partial f_i^{\mathrm{vis}}}{\partial\xi^j}\right)\delta\left(\frac{\partial\xi^j}{\partial x_i}\right)\mathrm{d}\Omega}_{F.S.D.}\\ &+\underbrace{\int_\Omega\left\{\mu\left[\frac{\partial u_i}{\partial\xi^k}\delta\left(\frac{\partial\xi^k}{\partial x_j}\right)+\frac{\partial u_j}{\partial\xi^k}\delta\left(\frac{\partial\xi^k}{\partial x_i}\right)\right]+\lambda\delta_{ij}\frac{\partial u_l}{\partial\xi^k}\delta\left(\frac{\partial\xi^k}{\partial x_l}\right)\right\}\left(\frac{\partial \Psi_{j+1}}{\partial x_i}+u_j\frac{\partial \Psi_m}{\partial x_i}\right)\mathrm{d}\Omega}_{F.S.D.}\\ &+\underbrace{\int_\Omega k\frac{\partial T}{\partial\xi^k}\delta\left(\frac{\partial\xi^k}{\partial x_i}\right)\frac{\partial \Psi_m}{\partial x_i}\mathrm{d}\Omega}_{F.S.D.}\end{aligned} \quad (47)$$

The field and boundary adjoint equations are the same as before and the final expression of the objective function gradient is

$$\begin{aligned}\delta F_{\mathrm{aug}} =& \frac{1}{2}\int_{S_w}(p-p_{\mathrm{tar}})^2\delta(\mathrm{d}S)+\int_{S_w}(\Psi_i p-\boldsymbol{\Psi}^{\mathrm{T}}\mathbf{f}_i)\delta(n_i\,\mathrm{d}S)\\ &+\int_{S_w}\Psi_m q_j\delta(n_j\,\mathrm{d}S)+\int_{S_w}\frac{\Psi_{i+1}}{n_i}\tau_{ij}\delta(n_i n_j)\mathrm{d}S\\ &+\int_\Omega\boldsymbol{\Psi}^{\mathrm{T}}\left(\frac{\partial f_i^{\mathrm{inv}}}{\partial\xi^j}-\frac{\partial f_i^{\mathrm{vis}}}{\partial\xi^j}\right)\delta\left(\frac{\partial\xi^j}{\partial x_i}\right)\mathrm{d}\Omega\\ &+\int_\Omega\left\{\mu\left[\frac{\partial u_i}{\partial\xi^k}\delta\left(\frac{\partial\xi^k}{\partial x_j}\right)+\frac{\partial u_j}{\partial\xi^k}\delta\left(\frac{\partial\xi^k}{\partial x_i}\right)\right]+\lambda\delta_{ij}\frac{\partial u_l}{\partial\xi^k}\delta\left(\frac{\partial\xi^k}{\partial x_l}\right)\right\}\left(\frac{\partial \Psi_{j+1}}{\partial x_i}+u_j\frac{\partial \Psi_m}{\partial x_i}\right)\mathrm{d}\Omega\\ &+\int_\Omega k\frac{\partial T}{\partial\xi^k}\delta\left(\frac{\partial\xi^k}{\partial x_i}\right)\frac{\partial \Psi_m}{\partial x_i}\mathrm{d}\Omega\end{aligned} \quad (48)$$

Note that Eq. (48) depends also on field variation.

6. Quasi-3D and rotational source terms

For quasi-3D or 3D flow equations within rotating domains, the extra terms denoted by $\mathbf{Q}$ or $\tau_{ij}^{\star}$ in Eqs. (1) and (2) (see expressions in Eqs. (4) and (5)) should be taken into account.

For the design of quasi-3D cascades, with variable streamtube thickness distribution, the variation in $\mathbf{Q}$ adds one more term to the field adjoint equations, Eq. (44), which read

$$\frac{\partial \boldsymbol{\Psi}}{\partial t}-A_i^{\mathrm{T}}\frac{\partial \boldsymbol{\Psi}}{\partial x_i}-M^{-T}\mathbf{K}=-\mathbf{Q}_\Psi \quad (49)$$

where the r.h.s. term stands for

$$\mathbf{Q}_\Psi=-\left(h\frac{\mathrm{d}h}{\mathrm{d}x_1}\right)\left[\Psi_2\frac{\partial p}{\partial\mathbf{U}}+\frac{2}{3}\mu\left(\Psi_2\frac{2}{h}\frac{\mathrm{d}h}{\mathrm{d}x_1}+\frac{\partial\Psi_2}{\partial x_1}\right)\frac{\partial u_1}{\partial\mathbf{U}}+\frac{2}{3}\mu\frac{\partial\Psi_2}{\partial x_2}\frac{\partial u_2}{\partial\mathbf{U}}\right] \quad (50)$$

The viscous term K_3 should also be modified due to the extra stress τ_{nn}, so that

$$K_3'=K_3-h\frac{\mathrm{d}h}{\mathrm{d}x_1}\left(\frac{\partial\Psi_i}{\partial x_i}+u_i\frac{\partial\Psi_m}{\partial x_i}\right) \quad (51)$$

and a new boundary integral term, namely

$$\int_{S_w}h\frac{\mathrm{d}h}{\mathrm{d}x_1}\frac{2}{3}\mu\Psi_2\frac{\partial u_i}{\partial x_k}\delta x_k n_i\,\mathrm{d}S \quad (52)$$

should be added to Eq. (46).

For the design of 3D rotating geometries, terms due to the rotation speed ω should be considered as well. In conformity with Eq. (49), the adjoint source term $\mathbf{Q}_\Psi$ should include terms such as

$$\mathbf{Q}_\Psi=\left[0,-2\omega\Psi_3-\omega^2x_1\Psi_1,2\omega\Psi_2-\omega^2x_2\Psi_1,0,0\right]^{\mathrm{T}} \quad (53)$$

7. Losses minimization—extension to field functionals

For the minimization of losses through 2D or 3D flow passages, the objective function can be defined as a field integral of the entropy generation [30], namely

$$F=\int_\Omega\rho u_i\frac{\partial s}{\partial x_i}\mathrm{d}\Omega \quad (54)$$

By applying the Gauss' divergence theorem, the field integral is transformed to a boundary one, which, stands for the difference in mass averaged entropy s between the inlet and outlet

$$F=\int_S\rho V_n s\,\mathrm{d}S=\int_{S_{i,o}}\rho V_n s\,\mathrm{d}S=\int_{S_o}s\,\mathrm{d}\dot{m}-\int_{S_i}s\,\mathrm{d}\dot{m} \quad (55)$$

Concerning only the entropy generation in viscous boundary layers, [30], Eq. (54) is expressed in terms of temperature and velocity gradients as

$$F=\int_\Omega\frac{1}{T}\tau_{ij}\frac{\partial u_i}{\partial x_j}\mathrm{d}\Omega \quad (56)$$

This is used as the objective function for losses minimization and the adjoint method is applied to compute its gradient. The function variation reads

$$\delta F=\int_\Omega\delta\left(\frac{1}{T}\tau_{ij}\frac{\partial u_i}{\partial x_j}\right)\mathrm{d}\Omega+\int_\Omega\frac{1}{T}\tau_{ij}\frac{\partial u_i}{\partial x_j}\delta(\mathrm{d}\Omega) \quad (57)$$

According to Appendix A, the variation of the finite volume $\delta(\mathrm{d}\Omega)$ is expressed in terms of $\mathrm{d}\Omega$ as

$$\delta(\mathrm{d}\Omega) = \frac{\partial(\delta x_k)}{\partial x_k}\mathrm{d}\Omega \tag{58}$$

Using Eq. (58), Eq. (12) for the variation in velocity gradient, Eq. (31) for stresses variation and by applying the Gauss' divergence theorem for the terms including gradients of the variation in both flow and geometrical quantities, the objective function variation finally reads

$$\begin{aligned}\delta F = &-\int_\Omega \frac{\mu}{T^2}R\left(\delta T - \frac{\partial T}{\partial x_i}\delta x_i\right)\mathrm{d}\Omega \\ &-\int_\Omega \frac{\partial}{\partial x_j}\left(\frac{\mu}{T}R_{ij}\right)\left(\delta u_i - \frac{\partial u_i}{\partial x_k}\delta x_k\right)\mathrm{d}\Omega \\ &-\int_{S_w}\frac{\mu}{T}R_{ij}\frac{\partial u_j}{\partial x_k}n_i\,\delta x_k\,\mathrm{d}S + \int_{S_w}\frac{\mu}{T}R\delta x_i n_i\,\mathrm{d}S \\ &+\int_{S_w}\frac{\mu}{T}R_{ij}n_j\,\delta u_i\,\mathrm{d}S\end{aligned} \tag{59}$$

where

$$R = \tau_{ij}\frac{\partial u_i}{\partial x_j}, \quad R_{ij} = 2(1+\delta_{ij})\frac{\partial u_i}{\partial x_j} + 2(1-\delta_{ij})\frac{\partial u_j}{\partial x_i} - \frac{4}{3}\delta_{ij}\frac{\partial u_k}{\partial x_k}$$

In this case, the variation in F_{aug} reads

$$\begin{aligned}\delta F_{\mathrm{aug}} = &\underbrace{-\int_\Omega \frac{\mu}{T^2}R\left(\delta T - \frac{\partial T}{\partial x_i}\delta x_i\right)\mathrm{d}\Omega}_{F.A.E.} \underbrace{-\int_\Omega \frac{\partial}{\partial x_j}\left(\frac{\mu}{T}R_{ij}\right)\left(\delta u_i - \frac{\partial u_i}{\partial x_k}\delta x_k\right)\mathrm{d}\Omega}_{F.A.E.} \\ &\underbrace{-\int_{S_w}\frac{\mu}{T}R_{ij}\frac{\partial u_j}{\partial x_k}n_i\,\delta x_k\,\mathrm{d}S}_{B.S.D} \underbrace{+\int_{S_w}\frac{\mu}{T}R\delta x_i n_i\,\mathrm{d}S}_{B.S.D.} \underbrace{+\int_{S_w}\frac{\mu}{T}R_{ij}n_j\,\delta u_i\,\mathrm{d}S}_{B.S.D.} \underbrace{-\int_\Omega\left(\delta\mathbf{U} - \frac{\partial\mathbf{U}}{\partial x_k}\delta x_k\right)^{\mathrm{T}}\left(A_i^{\mathrm{T}}\frac{\partial\boldsymbol{\Psi}}{\partial x_i}\right)\mathrm{d}\Omega}_{F.A.E.} \\ &\underbrace{-\int_\Omega\left(\delta\mathbf{W} - \frac{\partial\mathbf{W}}{\partial x_k}\delta x_k\right)^{\mathrm{T}}\mathbf{K}\,\mathrm{d}\Omega}_{F.A.E.} \underbrace{+\int_\Omega\boldsymbol{\Psi}^{\mathrm{T}}\frac{\partial}{\partial x_k}\left(\frac{\partial\mathbf{f}_i^{\mathrm{inv}}}{\partial x_j} - \frac{\partial\mathbf{f}_i^{\mathrm{vis}}}{\partial x_j}\right)\delta x_k\,\mathrm{d}\Omega}_{D.F.E.} \underbrace{-\int_{S_w}\frac{\partial\mathbf{U}^{\mathrm{T}}}{\partial x_k}(A_i^{\mathrm{T}}n_i)\boldsymbol{\Psi}\delta x_k\,\mathrm{d}S}_{B.S.D.} \\ &\underbrace{+\int_{S_w}\Psi_i n_i\delta p\,\mathrm{d}S}_{B.C.2} \underbrace{+\int_{S_w}(\Psi_i p - \boldsymbol{\Psi}^{\mathrm{T}}\mathbf{f}_i)\delta(n_i\,\mathrm{d}S)}_{B.S.D.} \underbrace{+\int_{S_{i,o}}\delta\mathbf{U}^{\mathrm{T}}(A_n^{\mathrm{T}}\boldsymbol{\Psi})\mathrm{d}S}_{B.C.3} \\ &\underbrace{+\int_{S_w}\delta u_i\left[\mu\left(\frac{\partial\Psi_{j+1}}{\partial x_i} + u_j\frac{\partial\Psi_m}{\partial x_i} + \frac{\partial\Psi_{i+1}}{\partial x_j} + u_i\frac{\partial\Psi_m}{\partial x_j}\right) + \lambda\delta_{ij}\left(\frac{\partial\Psi_{k+1}}{\partial x_k} + u_k\frac{\partial\Psi_m}{\partial x_k}\right) - \Psi_m\tau_{ij}\right]n_j\,\mathrm{d}S}_{B.C.4} \\ &\underbrace{+\int_{S_w}\delta T\left(k\frac{\partial\Psi_m}{\partial x_i}n_i\right)\mathrm{d}S}_{B.C.5} \underbrace{-\int_{S_w}\Psi_m\delta(q_j n_j\,\mathrm{d}S)}_{B.C.6} \underbrace{+\int_{S_w}\Psi_m q_j\delta(n_j\,\mathrm{d}S)}_{B.S.D.} \\ &\underbrace{-\int_{S_w}\frac{\Psi_{i+1}}{n_i}[\delta\tau_{ij}n_i n_j + \tau_{ij}\delta(n_i n_j)]\mathrm{d}S}_{B.C.7} \underbrace{+\int_{S_w}\frac{\Psi_{i+1}}{n_i}\tau_{ij}\delta(n_i n_j)\mathrm{d}S}_{B.S.D.} \underbrace{-\int_{S_w}u_i\Psi_m\delta\tau_{ij}n_j\,\mathrm{d}S}_{B.C.8} \\ &\underbrace{-\int_{S_w}\frac{\partial u_i}{\partial x_l}\left[\mu\left(\frac{\partial\Psi_{j+1}}{\partial x_i} + u_j\frac{\partial\Psi_m}{\partial x_i} + \frac{\partial\Psi_{i+1}}{\partial x_j} + u_i\frac{\partial\Psi_m}{\partial x_j}\right) + \lambda\delta_{ij}\left(\frac{\partial\Psi_{k+1}}{\partial x_k} + u_k\frac{\partial\Psi_m}{\partial x_k}\right)\right]\delta x_l n_j\,\mathrm{d}S}_{B.S.D.} \\ &\underbrace{+\int_{S_w}\frac{\partial T}{\partial x_k}\left(k\frac{\partial\Psi_m}{\partial x_i}\right)\delta x_k n_i\,\mathrm{d}S}_{B.S.D} \underbrace{-\int_{S_w}\left(\boldsymbol{\Psi}^{\mathrm{T}}\frac{\partial\mathbf{f}_i^{\mathrm{vis}}}{\partial x_k}\right)\delta x_k n_i\,\mathrm{d}S}_{B.S.D.}\end{aligned} \tag{60}$$

The field adjoint equations are written as

$$\frac{\partial\boldsymbol{\Psi}}{\partial t} - A_i^{\mathrm{T}}\frac{\partial\boldsymbol{\Psi}}{\partial x_i} - M^{-T}\mathbf{K} - M^{-T}\mathbf{L} = \mathbf{0} \tag{61}$$

where

$$L_1 = \frac{1}{T^2}R\left(-\frac{p}{\rho^2(\gamma-1)}\right)$$

$$L_{i+1} = \frac{\partial}{\partial x_j}\left(\frac{\mu}{T}R_{ij}\right)$$

$$L_m = \frac{1}{T^2}R\frac{1}{\rho(\gamma-1)}$$

The adjoint boundary conditions are the same with the viscous inverse design case except for the adjoint "velocity" terms for which $\Psi_{i+1} = 0$, $i = 1, 2(3)$.

After satisfying of the field and boundary adjoint equations, the remaining terms express the gradient of the objective function as follows:

$$\begin{aligned}\delta F_{\mathrm{aug}} = &\int_{S_w}\frac{\mu}{T}R_{ij}\frac{\partial u_j}{\partial x_k}n_i\,\delta x_k\,\mathrm{d}S + \int_{S_w}\frac{\mu}{T}R\,\delta x_i n_i\,\mathrm{d}S \\ &+\int_{S_w}\frac{\mu}{T}R_{ij}n_j\,\delta u_i\,\mathrm{d}S + \int_{S_w}(\Psi_i p - \boldsymbol{\Psi}^{\mathrm{T}}\mathbf{f}_i)\delta(n_i\,\mathrm{d}S) \\ &-\int_{S_w}\frac{\partial\mathbf{U}^{\mathrm{T}}}{\partial x_k}(A_i^{\mathrm{T}}n_i)\boldsymbol{\Psi}\,\delta x_k\,\mathrm{d}S + \int_{S_w}\left(\boldsymbol{\Psi}^{\mathrm{T}}\frac{\partial\mathbf{f}_{vi}}{\partial x_k}\right)\delta x_k n_i\,\mathrm{d}S \\ &+\int_{S_w}\frac{\Psi_{i+1}}{n_i}\tau_{ij}\delta(n_i n_j)\mathrm{d}S + \int_{S_w}\Psi_m q_j\delta(n_j\,\mathrm{d}S) \\ &-\int_{S_w}\frac{\partial u_i}{\partial x_l}\left[\mu\left(\frac{\partial\Psi_{j+1}}{\partial x_i} + u_j\frac{\partial\Psi_m}{\partial x_i} + \frac{\partial\Psi_{i+1}}{\partial x_j} + u_i\frac{\partial\Psi_m}{\partial x_j}\right)\right. \\ &\left.+\lambda\delta_{ij}\left(\frac{\partial\Psi_{k+1}}{\partial x_k} + u_k\frac{\partial\Psi_m}{\partial x_k}\right)\right]\delta x_l n_j\,\mathrm{d}S\end{aligned} \tag{62}$$

It is important that no field terms appear in Eq. (62), although the functional to be minimized is a field integral over the whole computational domain.

8. Results and discussion

In this section, the validation of the proposed method is carried out using a number of demonstration problems including the inverse design (shape reconstruction based on target pressure distributions) and optimization of isolated airfoils, 2D/3D turbomachinery cascades and an elbow duct. The analysis tool is a time-marching Euler/Navier–Stokes equations solver for structured or adaptive unstructured grids, based on the finite-volume technique and an upwind formulation. It employs the Roe's approximate Riemann solver [31] with variables' extrapolation to account for second-order accuracy. The van Leer–van Albada limiter [32] is utilized whenever deemed necessary, such as in the presence of extremely stretched grid cells. The Spalart–Allmaras model [33], is used for the turbulent flow cases; the turbulent viscosity coefficient variation is neglected during the development of the adjoint formulation. Bezier polynomials (for curves in 2D or surfaces in 3D) are used to parameterize each side of airfoils or blades.

In the transonic case examined, the unstructured grid is automatically adapted to the flow field during the pseudo-time integration. Local time-stepping is used in both the flow and adjoint equations. Within the first iterations, the CFL number used in the flow equations gradually reaches its maximum value determined by stability criteria and, afterwards, it remains constant; the maximum CFL number value attained during the solution of the flow equations is fixed and used for the adjoint equations. At the beginning of each cycle, a fast remeshing process is used for the current geometry. The steepest descent algorithm, with constant step size, is employed.

On some of the 2D problems, parametric studies have been carried out in order to shed light into the role of some parameters. Among them, issues related to the required degree of convergence of the direct and adjoint equations solver or on the effect of grid size to the accurate computation of the objective function gradient are discussed.

In the shape reconstruction cases, an existing airfoil or blade geometry (which will be referred to as the target or reference geometry) is first used to compute the target pressure coefficient distribution, at specified flow conditions. The existence of reference geometries allows comparisons to be made not only between the target pressure distributions and that computed over the optimal airfoil but also between optimal and reference geometries.

8.1. Inviscid airfoil reconstructions

8.1.1. Subsonic and transonic isolated airfoil reconstruction

In the first example, the RAE2822 airfoil is used as reference geometry. Two problems based on the same reference isolated airfoil are analyzed; the flow is subsonic with $M_\infty = 0.5$ and $a_\infty = 3°$ (first problem) and transonic with $M_\infty = 0.73$, $a_\infty = 3.19°$ (second). The same initial control point distribution is used in both cases, with 15 control points on either airfoil side. The unstructured grid allows two refinements during the solution of the Euler equations at transonic flow conditions. In each cycle, the grid obtained at the end of the solution of the direct problem is, then, used to solve the adjoint equations. For the transonic flow problem, the final grid around the optimal airfoil shape as well as the corresponding Mach number field is illustrated in Fig. 1. Fig. 2 compares the starting, target and optimal-computed airfoil shapes along with the corresponding C_p distribution. The convergence of the objective function is plotted in Fig. 3, for both cases. We may notice the good performance of the method even in the presence of a "purposely" non-continuous (due to the presence of the shock) target pressure distribution.

In both cases, the comparison between target and optimal pressure coefficients and shapes is excellent. In the transonic case, in which the van Leer–van Albada limiter is activated only for the flow equations, the shock is computed at the same location and with the same strength as in the reference geometry. The leading edge radius is correctly captured, too; in order to achieve a rounded leading

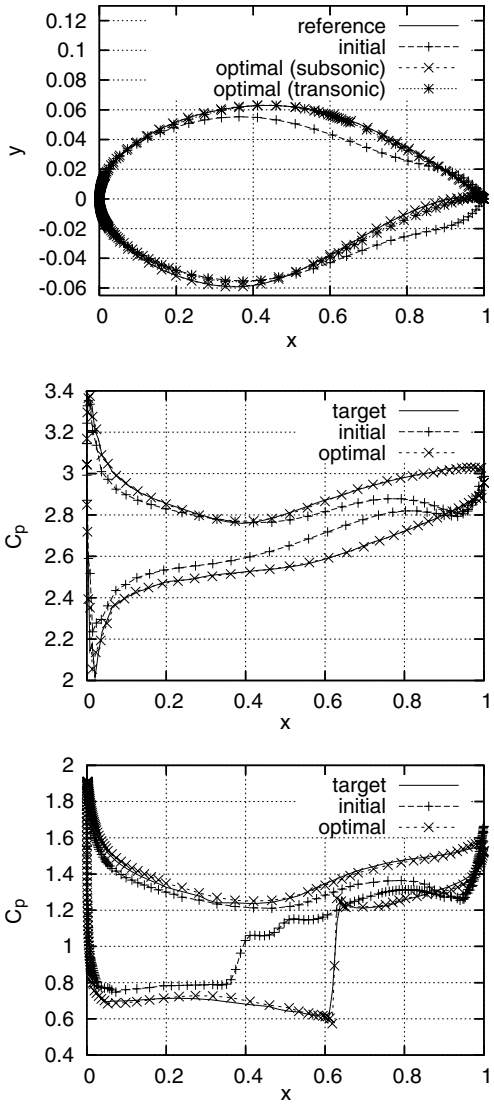

Fig. 2. Isolated airfoil reconstruction; inviscid, transonic and subsonic flow. Initial, optimal and reference airfoils (top), corresponding C_p distributions for the subsonic (middle) and transonic (bottom) flow problems.

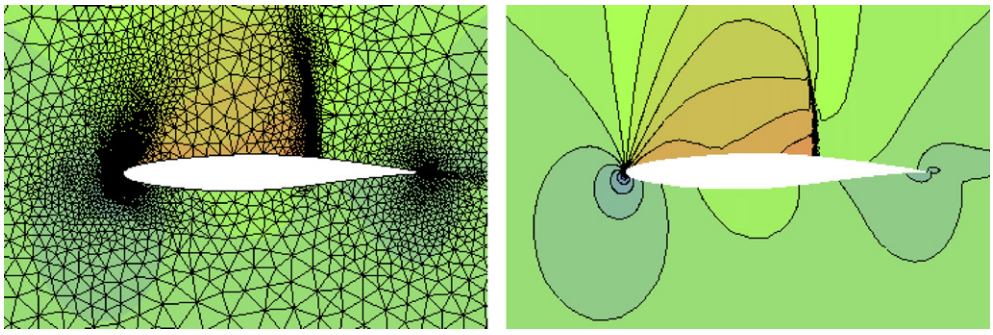

Fig. 1. Isolated airfoil reconstruction; inviscid, transonic flow. Left: Unstructured grid adapted to the flow; right: Mach number distribution around the optimal airfoil. Maximum Mach = 1.64, increment = 0.07.

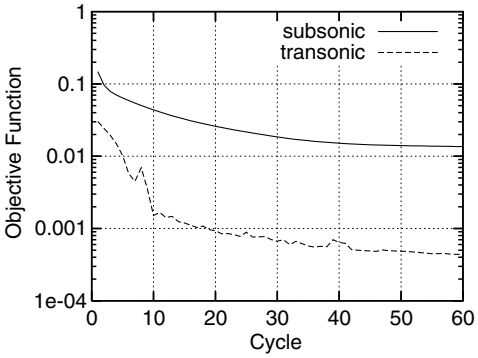

Fig. 3. Isolated airfoil reconstruction; inviscid, transonic and subsonic flow. Convergence of the steepest descent algorithm.

edge with curvature continuity, the starting and its two adjacent control points are restricted to lie on the same straight line. About 60 cycles are enough for the optimal airfoil to be computed; slight disturbances that occur afterwards, in the transonic flow problem, are due to the presence of discontinuity in the target which is very sensitive even to the slightest changes in shape. The different final level of objective function values in the two cases examined should not lead us to any comparative argument.

8.1.2. Quasi-3D compressor airfoil reconstruction

The next example is the reconstruction of a 2D compressor cascade, at inviscid flow conditions ($M_{\text{out,is}} = 0.4$ and $a_{\text{in}} = 50°$). The suction and pressure airfoil sides are parameterized using 11 Bezier control points each, at zero stagger angle. All internal control points are fixed at preset chordwise stations giving, thus, rise to a single degree of freedom per control point. An H-type structured grid is used. The case is examined with non-unit axial-velocity–density-ratio (AVDR = 0.9) which results to a quasi-3D flow field with streamtube thickness varying linearly between the leading and trailing edges. In Fig. 4, the comparison of the reference geometry and C_p distribution to the optimal ones is shown; the comparison is very satisfactory. The convergence of the objective function is shown in Fig. 5; a reduction of about four orders of magnitude is achieved within the first 100 cycles. A slow degradation in the objective function value during the subsequent 400 cycles, without significantly changing the optimal airfoil shape is observed; so one may consider that 100 cycles are, in fact, enough to reconstruct the target C_p distribution.

In Fig. 6, the sensitivity derivatives computed through the numerical solution of the adjoint equations, on the starting geometry, are compared with the same quantities approximated using finite-difference schemes. The two curves are in good agreement with slight discrepancies close to the leading and trailing edges, where the use of an H-type grid leads to skewed mesh cells.

Some elsewhere published statements [23], on substantially different requirements concerning the convergence of the direct and adjoint equations are reconfirmed in

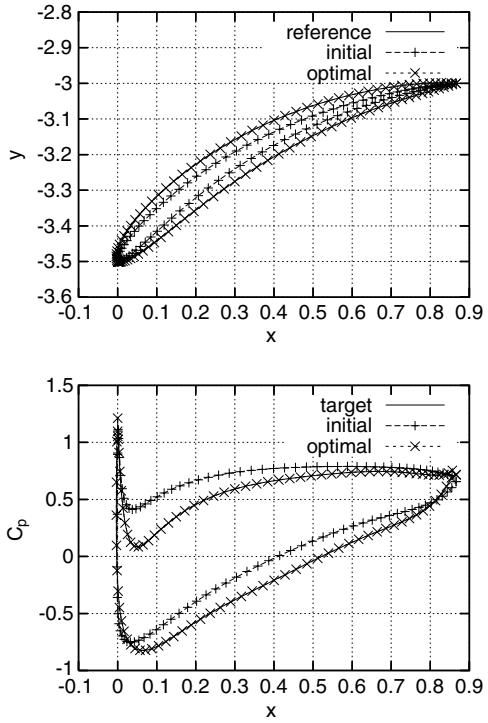

Fig. 4. Quasi-3D compressor airfoil reconstruction; inviscid flow. Top: initial, optimal and target geometry; bottom: initial, optimal and target C_p distribution.

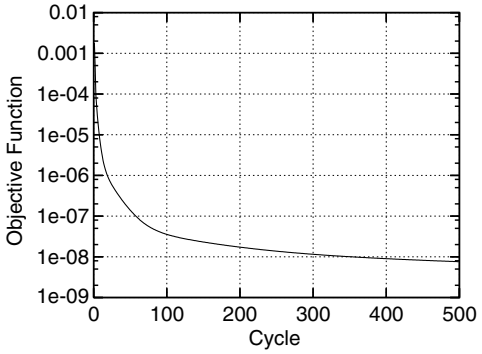

Fig. 5. Quasi-3D compressor airfoil reconstruction; inviscid flow. Convergence of the steepest descent algorithm.

Fig. 7. In this figure, the objective function derivatives are computed with different levels of convergence for the flow and adjoint equations. It is obviously meant that in the first study (Fig. 7, top) the adjoint equations converged to machine accuracy whereas the same holds for the flow equations in the second study (Fig. 7, bottom). Consequently, the convergence criterion for the adjoint equations can be relaxed since, as it can be seen from this figure, the convergence of these equations by just a few orders of magnitude seems to be adequate. The same case is examined three times, with three different structured grids. According to Fig. 8, the gradient components computed using a 163×41 or 219×61 H-type grid are almost identical, which signifies that grid independent solutions are obtained.

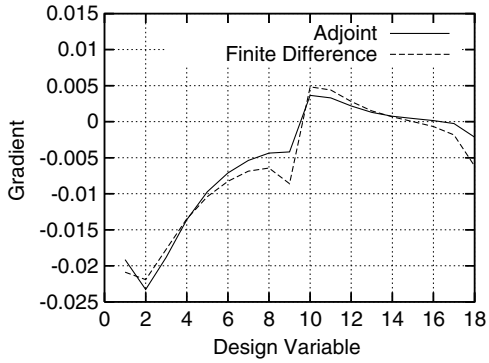

Fig. 6. Quasi-3D compressor airfoil reconstruction; inviscid flow. Objective function gradient components computed using the adjoint method and the finite-difference scheme. The first half of the abscissas correspond to the suction side and the rest of them to the pressure side (both measured from the leading to the trailing edge).

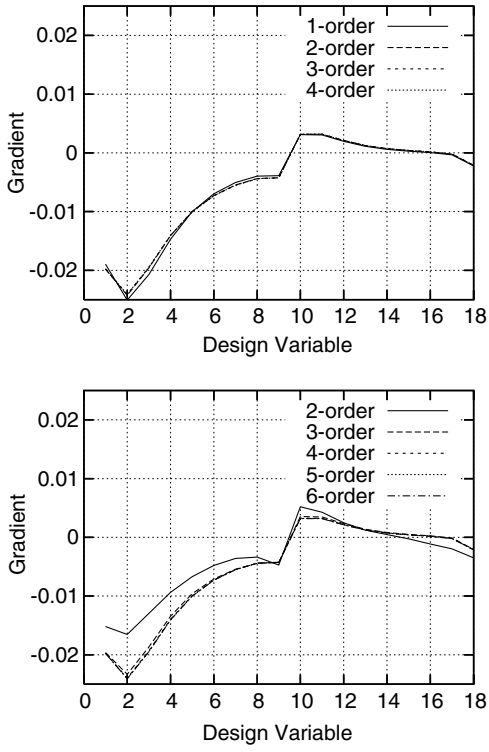

Fig. 7. Quasi-3D compressor airfoil reconstruction; inviscid flow. Comparison of the objective function gradient components computed using different levels of convergence of the direct (top; adequately converged adjoint equations) and the adjoint equations (bottom; adequately converged flow equations).

8.2. Inviscid 3D blade reconstructions

8.2.1. Reconstruction of a 3D compressor blade

The next problem examined is that of the inverse design of a 3D compressor rotor blade that reproduces a given pressure distribution over its suction and pressure surfaces. The isentropic Mach number at the outlet hub is equal to $M_{\text{out,is}} = 0.4$ and the peripheral and radial inlet flow angles

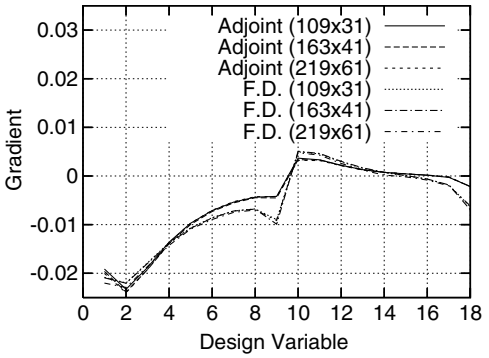

Fig. 8. Quasi-3D compressor airfoil reconstruction; inviscid flow. Comparison of the objective function gradient components computed using the adjoint equations and finite-differences (F.D.) for various mesh sizes.

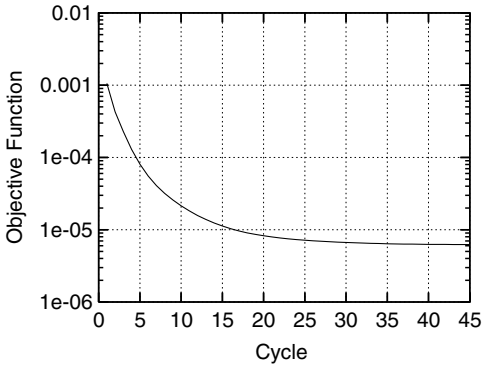

Fig. 9. 3D compressor rotor blade reconstruction; inviscid flow. Convergence of the steepest descent algorithm.

are $a_{\text{per}} = 58°$, $a_{\text{rad}} = 0°$. The blade surfaces are parameterized using Bezier surfaces with $4 \times 5 = 20$ control points on each blade side (4 in the radial and 5 in the axial direction). The leading and trailing edge control points are kept constant. The remaining control points have fixed projections on the meridional plane and are allowed to vary only in the peripheral direction, resulting to 24 design variables in total. In this case, the steepest descent method, driven by the derivatives computed by the adjoint method, converged about two orders of magnitude within approximately 50 cycles, Fig. 9. The control point location and the initial and optimal geometry and Mach number distribution are illustrated in Fig. 10.

8.2.2. Reconstruction of a 3D turbine blade

Similar results are shown for the second 3D case dealing with the inverse design of a 3D peripheral turbine cascade, for inviscid flow conditions. The blade surfaces are parameterized using two Bezier surfaces with 3×10 (in the radial and axial direction, respectively) control points each. The axial and peripheral components of the internal control points are allowed to vary (the leading and trailing edge points are kept constant), resulting to $2 \times 2 \times 3 \times 8 = 96$ design variables in total. The 3D Euler and the corresponding adjoint equations are solved after generating an H-type

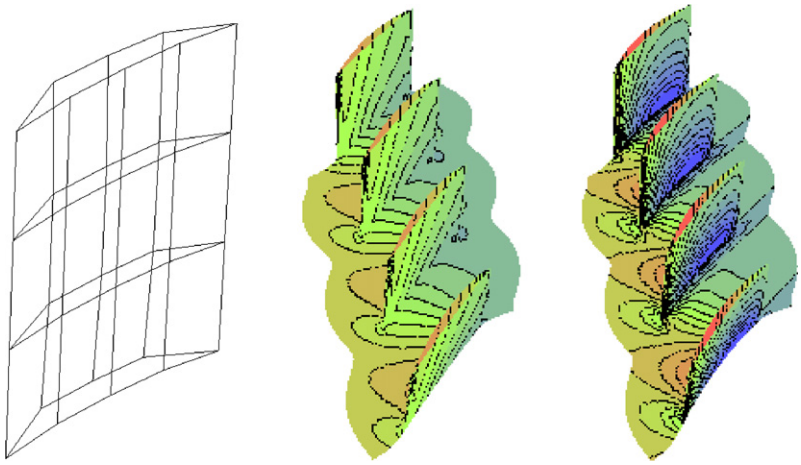

Fig. 10. 3D compressor rotor blade reconstruction; inviscid flow. The grid of control points (left) and the Mach number distributions maximum Mach number = 1.01 on the initial (middle) and optimal (right) blade. The latter is almost identical to the target distribution which is not repeated here.

structured grid with approximately 12,000 nodes. In Fig. 11, the Mach number distribution over cascades, with the initial and optimal blades, are shown. The Mach number distribution on the optimal blade perfectly matches the target one. Fig. 12 illustrates the convergence of the optimization method. The steepest descent method converges within 80 cycles. The pressure distribution at the blade midspan is shown for the target, initial and optimal geometry in Fig. 13, while the comparison between finite-differences and the adjoint sensitivities is depicted in Fig. 14. Both comparisons are very satisfactory.

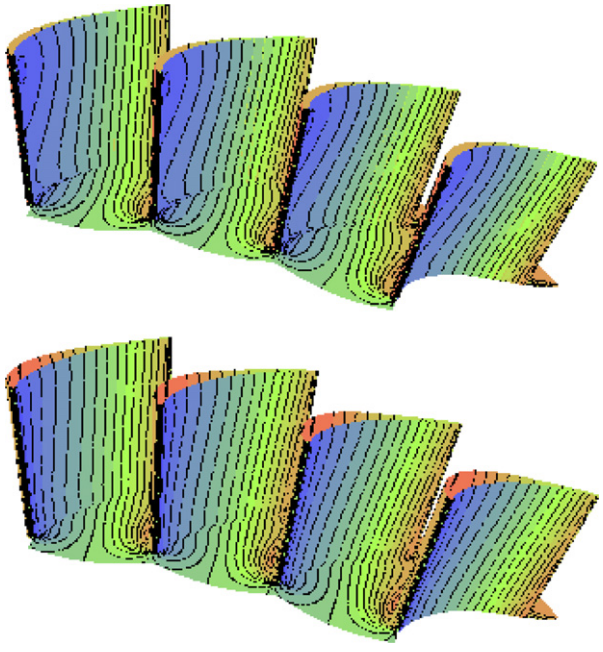

Fig. 11. 3D turbine stator blade reconstruction; inviscid flow. Mach number distribution on the initial (top) and optimal (bottom) blade surface and the hub. The optimal distribution is almost identical to the target one (not repeated here). The different initial and optimal blade shapes can be seen.

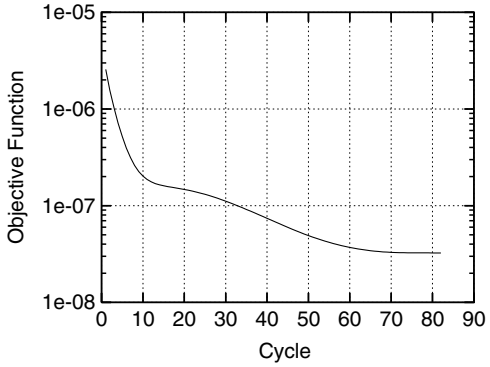

Fig. 12. 3D turbine stator blade reconstruction; inviscid flow. Convergence of the steepest descent algorithm.

8.3. Viscous 2D airfoil reconstruction

8.3.1. Cascade reconstruction, laminar flow

The first example used to validate the viscous adjoint formulation is the inverse design of a plane cascade with laminar flow conditions, $M_{\text{out,is}} = 0.3$, $a_{\text{in}} = 30°$ and $Re = 1000$. Twelve Bezier control points are used for the parameterization of each airfoil side. The steepest descent method converges about two orders of magnitude within almost 160 cycles, Fig. 15, reproducing the desired target shape and pressure distribution, as shown in Fig. 16. The comparison between the gradient components computed with the adjoint method (proposed and traditional one) and those computed by a central finite-difference scheme is shown in Fig. 17.

8.3.2. Compressor cascade reconstruction, turbulent flow

The last case concerns the turbulent design of a 2D compressor cascade, $M_{\text{out,is}} = 0.3$, $a_{\text{in}} = 47°$ and $Re = 10^7$. The Spalart–Allmaras turbulence model is used. The blade is parameterized using 15 Bezier control points for each side. An H-type grid with 315×151 nodes is used. The method

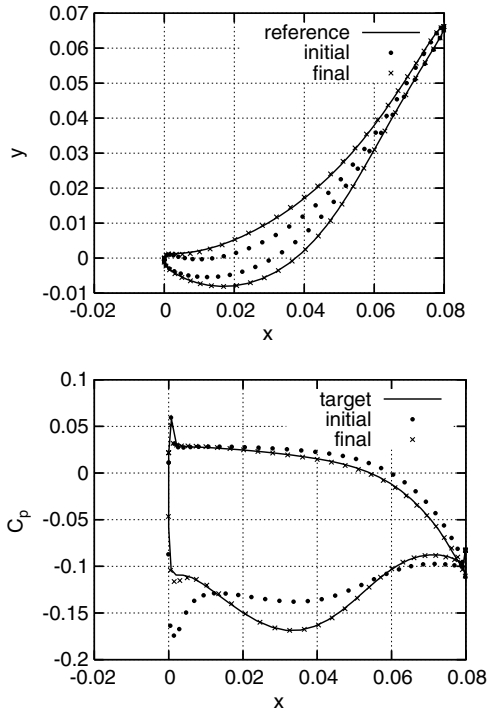

Fig. 13. 3D turbine stator blade reconstruction; inviscid flow. Target, initial and optimal geometry (top) and C_p distribution (bottom), at midspan.

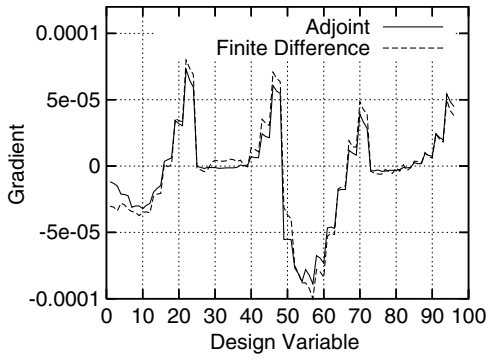

Fig. 14. 3D turbine stator blade reconstruction; inviscid flow. Objective function gradient components computed using the adjoint method and a finite-difference scheme.

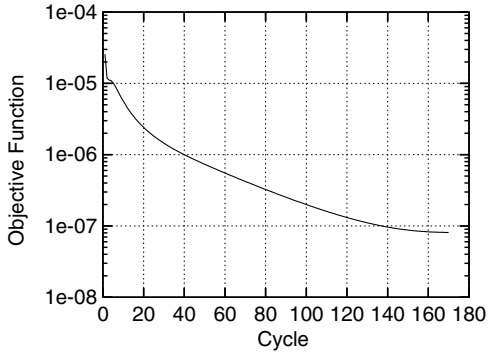

Fig. 15. Cascade airfoil reconstruction; laminar flow. Convergence of the steepest descent algorithm.

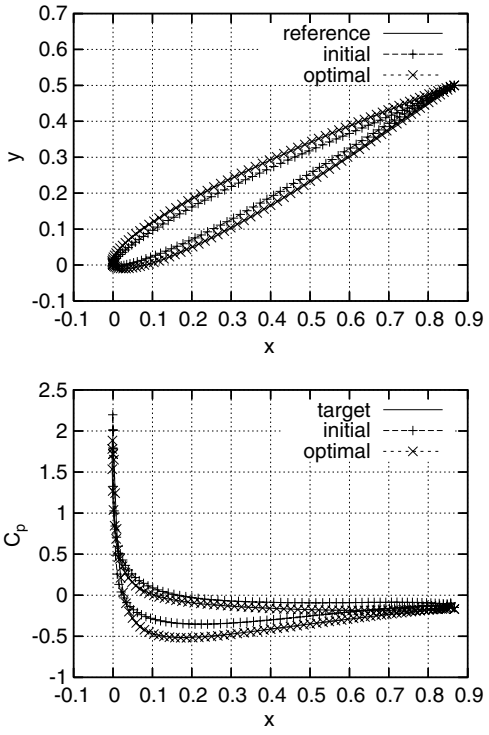

Fig. 16. Cascade airfoil reconstruction; laminar flow. Top: initial, optimal and target geometry, bottom: initial, optimal and target C_p distribution.

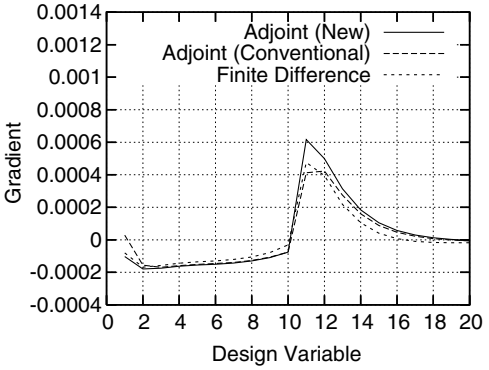

Fig. 17. Cascade airfoil reconstruction; laminar flow. Objective function gradient components computed using (a) the adjoint method and (b) a finite-difference scheme.

converges about 3.5 orders of magnitude within 140 cycles, Fig. 18, reproducing the target pressure distribution, Fig. 19.

8.4. Viscous losses minimization problems

8.4.1. Optimization of a 3D elbow duct, laminar flow

The next problem concerns the entropy generation minimization through a 3D elbow duct. The flow is considered laminar with $M_{\text{out,is}} = 0.4$, $Re = 10^3$ and $a_{\text{in}} = 0$. The elbow part of the duct is parameterized using nine Bezier control points for each side, from which only five per side are allowed to vary. All variable control points are restricted to move within a predefined orthogonal space. They are obliged to stay at the border of this space if the descent

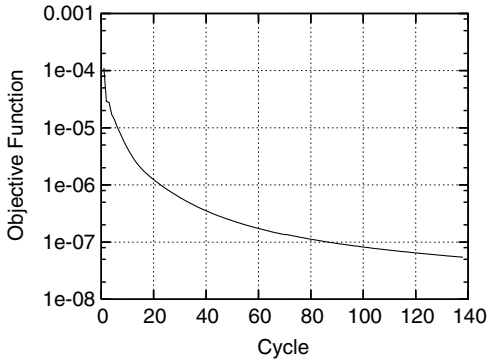

Fig. 18. Quasi-3D compressor airfoil reconstruction; turbulent flow. Convergence of the steepest descent algorithm.

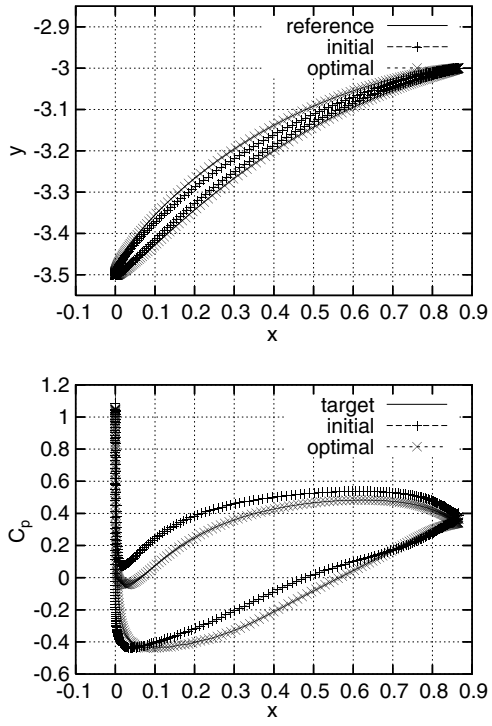

Fig. 19. Quasi-3D compressor airfoil reconstruction; turbulent flow. Top: initial, optimal and target geometry, bottom: initial, optimal and target C_p distribution.

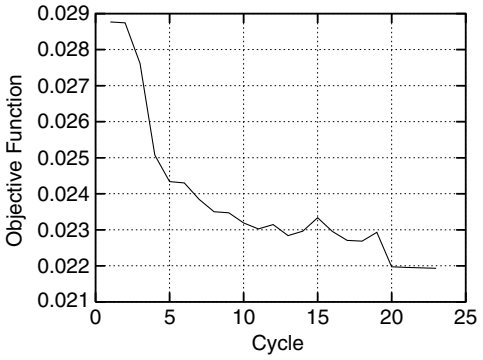

Fig. 20. 3D elbow duct optimization; laminar flow. Convergence of the steepest descent algorithm.

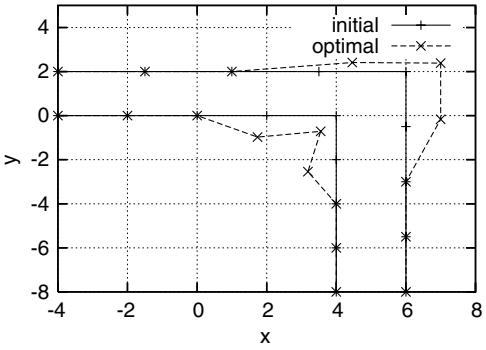

Fig. 21. 3D elbow duct optimization; laminar flow. Initial and optimal set of control points at midspan.

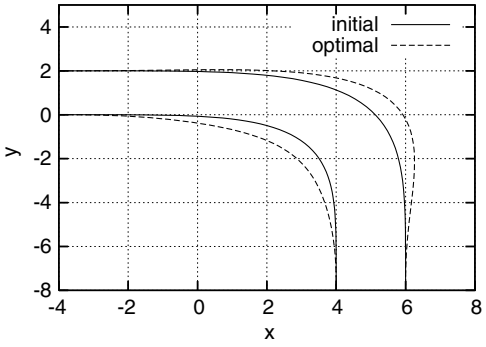

Fig. 22. 3D elbow duct optimization; laminar flow. Initial and optimal elbow geometry at midspan.

algorithm tends to drive them outside. The total pressure loss coefficient is reduced from $\omega = 0.062$ to $\omega = 0.048$ within 25 cycles according to the convergence plot of Fig. 20 showing the reduction in the overall entropy generation. The oscillations that appear are due to the constraints imposed for the control points.

Fig. 21 shows the initial and optimal set of control points, and Fig. 22 shows the corresponding duct geometries projected on the (x, y) plane. It is quite obvious that the duct tends to become thicker and the width of the optimal duct is limited by the user-defined search spaces for the control points.

In Fig. 23 a view of the 3D structured grid together with the pressure distribution over the wall is shown.

8.4.2. 3D compressor cascade optimization, turbulent flow

The final application is the optimization of a 3D peripheral compressor cascade in turbulent flow. The flow conditions are: axial inlet flow, $M_{\text{out,is}} = 0.5$ and $Re = 5 \times 10^5$. $5 \times 13 = 65$ control points are used to parameterize each blade side. Only the $R\theta$ components of the hub and tip control points are considered as free variables making a total of 28 design variables. The remaining control points are obtained by using linear interpolation. The cascade consists of 61 blades with fixed stagger angle of 27° and the H-type structured grid contains $191 \times 55 \times 71 = 745{,}855$ nodes.

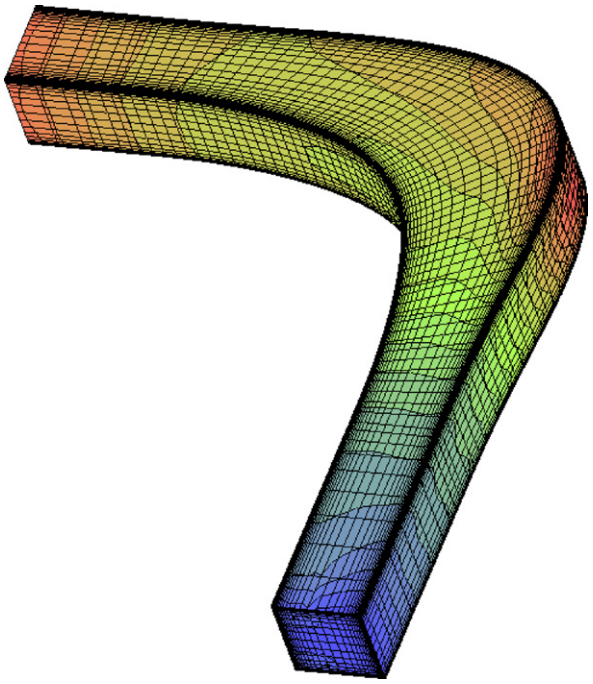

Fig. 23. 3D elbow duct optimization; laminar flow. 3D structured grid and pressure distribution.

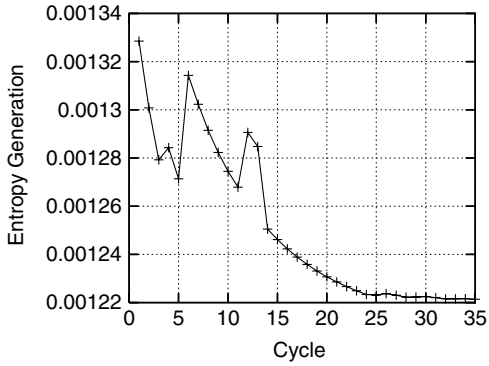

Fig. 24. 3D compressor cascade optimization; turbulent flow. Convergence of entropy generation rate.

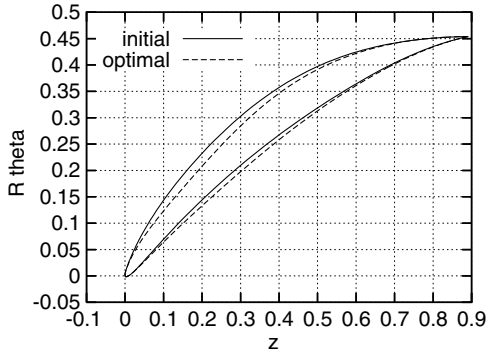

Fig. 25. 3D compressor cascade optimization; turbulent flow. Initial and optimal blade contours at hub.

The convergence of the entropy generation function is shown in Fig. 24. The oscillations occurring during the optimization cycles are due to the constraint imposition. In order to deal with the geometrical inequality constraints for the minimum allowed thickness, a penalty coefficient and additional Lagrange multipliers are introduced and the inequality constrained problem is transformed to an equality constrained one and, then, to an unconstrained one. The total pressure losses' coefficient decreases from $\omega = 0.038$ to $\omega = 0.033$. The blade contours for the hub and the tip of the initial and the optimal blade are shown in Figs. 25 and 26. In Fig. 27, the pressure distribution for the optimal 3D geometry is illustrated.

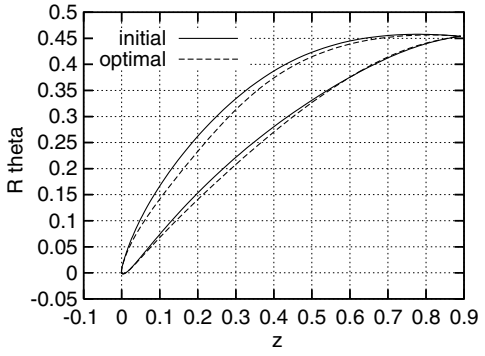

Fig. 26. 3D compressor cascade optimization; turbulent flow. Initial and optimal blade contours at tip.

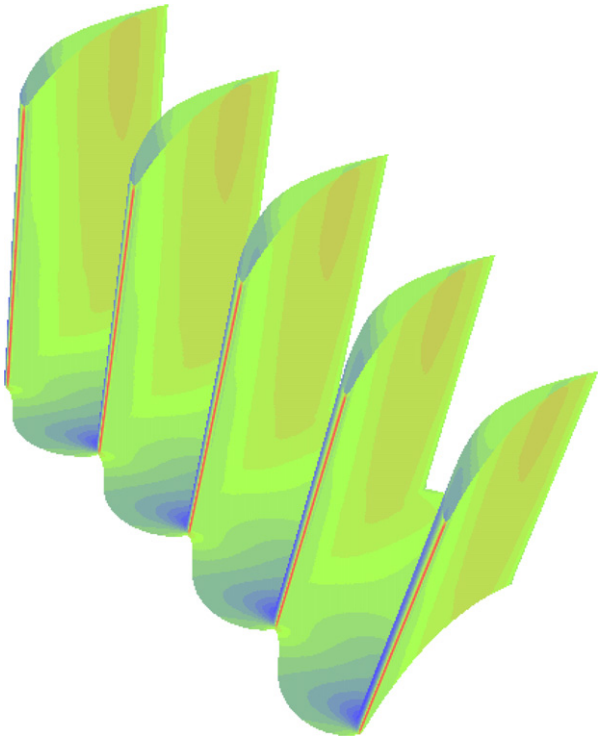

Fig. 27. 3D compressor cascade optimization; turbulent flow. Mach number distribution over the blade and hub surfaces of the optimal peripheral cascade. Minimum $P = 1.4$ bar, maximum $P = 2.5$ bar, increment $= 0.055$ bar.

9. Conclusions

A continuous adjoint method for the design and optimization of 2D or 3D aerodynamic shapes was presented. An important feature of the proposed formulation is that the computation of the objective function gradient is exclusively based on boundary integrals; this is feasible for objective functions based on either boundary or field integrals. To convince the reader, both inverse design and shape optimization problems where a field integral of entropy generation terms is to be minimized have been presented. Field terms have been eliminated through the application of the Gauss' divergence theorem to the integral of the gradient of coordinate variations, resulted from the careful treatment of the variation in gradient. In the paper, it has been demonstrated that the computation of these terms using the variations in grid metrics (a computation which is feasible only for structured grids) leads to identical results. The elimination of field terms leads to CPU cost reduction with the same accuracy, as guaranteed by comparing the gradient values obtained using the traditional and the proposed method with those obtained using finite differences. The objective function gradient can be computed through the same formulas, regardless of the grid type; this is why structured or unstructured grids can be used. The proposed method is valid for both inviscid and viscous flows, in stationary and rotating frames. A transonic case has been examined too. The viscous adjoint equations have been derived by carrying out a second integration by parts, to both flow and geometrical variations. The elimination of field integrals is, of course, valid in viscous flows as well. The steepest descent algorithm has been successfully used to reconstruct/optimize 2D or 3D shapes within a reasonable number of cycles.

Acknowledgement

The first author was supported by a grant from the Beneficial Foundation Alexandros S. Onasis.

Appendix A. Metrics variation

On a body-fitted structured grid, the contravariant and covariant transformation metrics are defined as

$$\nabla\xi^i = \frac{1}{2J}(\mathbf{r}_{,j}\times\mathbf{r}_{,k})e_{ijk}, \quad \mathbf{r}_{,i} = \frac{1}{2}J(\nabla\xi^j\times\nabla\xi^k)e_{ijk} \tag{63}$$

where e_{ijk} is the permutation symbol and $J=\mathbf{r}_{,i}(\mathbf{r}_{,j}\times\mathbf{r}_{,k})$ is the Jacobian determinant of the transformation matrix $\left[\frac{\partial x_i}{\partial\xi^j}\right]$. The variation of the contravariant metrics yields

$$\delta(\nabla\xi^i) = \frac{1}{2J}(\delta\mathbf{r}_{,j}\times\mathbf{r}_{,k})e_{ijk} + \frac{1}{2J}(\mathbf{r}_{,j}\times\delta\mathbf{r}_{,k})e_{ijk} - \frac{\delta J}{2J^2}(\mathbf{r}_{,j}\times\mathbf{r}_{,k})e_{ijk} \tag{64}$$

The three terms on the r.h.s. of Eq. (64) are further developed with the help of Eqs. (63) to get

$$\frac{1}{2J}(\delta\mathbf{r}_{,j}\times\mathbf{r}_{,k})e_{ijk} = \nabla\xi^i(\delta\mathbf{r}_{,j}\nabla\xi^j) - \nabla\xi^j(\delta\mathbf{r}_{,j}\nabla\xi^i) \tag{65}$$

$$\frac{1}{2J}(\mathbf{r}_{,j}\times\delta\mathbf{r}_{,k})e_{ijk} = \nabla\xi^i(\delta\mathbf{r}_{,k}\nabla\xi^k) - \nabla\xi^k(\delta\mathbf{r}_{,k}\nabla\xi^i) \tag{66}$$

$$-\frac{\delta J}{2J^2}(\mathbf{r}_{,j}\times\mathbf{r}_{,k})e_{ijk} = -\nabla\xi^i(\delta\mathbf{r}_{,m}\nabla\xi^m) \tag{67}$$

Upon substitution of Eqs. (65)–(67) into Eq. (64), one gets

$$\delta(\nabla\xi^i) = -\nabla\xi^i(\delta\mathbf{r}_{,i}\nabla\xi^i) - \nabla\xi^j(\delta\mathbf{r}_{,j}\nabla\xi^i) - \nabla\xi^k(\delta\mathbf{r}_{,k}\nabla\xi^i) \tag{68}$$

and after some rearrangements

$$\delta\left(\frac{\partial\xi^i}{\partial x_j}\right) = -\frac{\partial\xi^i}{\partial x_k}\frac{\partial(\delta x_k)}{\partial x_j} \tag{69}$$

References

[1] Kampolis IC, Papadimitriou DI, Giannakoglou KC. Evolutionary optimization using a new radial basis function network and the adjoint formulation. J Inverse Probl Sci Eng, in press.
[2] Pironneau O. Optimal shape design for elliptic systems. New York: Springer-Verlag; 1984.
[3] Jameson A. Aerodynamic design via control theory. J Sci Comput 1988;3:33–260.
[4] Jameson A. Optimum aerodynamic design using CFD and control theory. AIAA paper 95-1729-CP, 1995.
[5] Jameson A, Nadarajah S, Alonso JJ. An adjoint method for the calculation of remote sensitivities in supersonic flow. AIAA paper 2002-0261, 30th AIAA aerospace sciences meeting, Reno, NV, January 2002.
[6] Nadarajah SK, Kim S, Jameson A, Alonso JJ. Sonic boom reduction using an adjoint method for supersonic transport aircraft configuration. In: Symposium transsonicum IV, International Union of Theoretical and Applied Mechanics, September 2–6, 2002, DLR Gottingen, Germany.
[7] Campobasso MS, Duta M, Giles MB. Adjoint methods for turbomachinery design. In: ISABE conference, Bangalore, 2001.
[8] Duta M, Giles MB, Campobasso MS. The harmonic adjoint approach to unsteady turbomachinery design. In: ICFD conference, Oxford, 2001.
[9] Campobasso MS, Duta M, Giles MB. Adjoint calculation of sensitivities of turbomachinery objective functions. AIAA J Propulsion Power 2003;19(4).
[10] Ferlauto M, Iollo A, Zannetti L. Optimal inverse method for turbomachinery design. In: ECCOMAS, Barcelona, 2000.
[11] Jameson A, Reuther J. Control theory based airfoil design using the euler equations. AIAA paper 94-4272-CP, 1994.
[12] Jameson A, Alonso JJ, Reuther JJ, Martinelli L, Vassberg JC. Aerodynamic shape optimization techniques based on control theory. AIAA paper 98-2538, 1998.
[13] Jameson A, Pierce N, Martinelli L. Optimum aerodynamic design using the Navier–Stokes equations. J Theor Comput Fluid Mech 1998;10:213–37.
[14] Anderson WK, Venkatakrishnan V. Aerodynamic design optimization on unstructured grids with a continuous adjoint formulation. Comput Fluids 1999;28:443–80.
[15] Giles MB. An introduction to the adjoint approach to design, ERCOFTAC workshop on adjoint methods, Toulouse, June 21–23, 1999.

[16] Giles MB. Adjoint methods for aeronautical design. In: ECCOMAS CFD conference, 2001.
[17] Nadarajah S, Jameson A. A comparison of the continuous and discrete adjoint approach to automatic aerodynamic optimization. AIAA paper 2000-0667, AIAA 38th Aerospace Sciences Meeting and Exhibit, Reno, NV, January 2000.
[18] Nadarajah S, Jameson A. Studies of the continuous and discrete adjoint approaches to viscous automatic aerodynamic optimization, AIAA paper 2001-2530. In: AIAA 15th computational fluid dynamics conference, Anaheim, CA, June 2001.
[19] Giles MB, Pierce NA. Adjoint equations in CFD: duality, boundary conditions and solution behaviour. AIAA paper 97-1850, 1997.
[20] Giles MB, Pierce NA. On the properties of solutions of the adjoint Euler equations. In: ICFD conference, Oxford, 1998.
[21] Giles MB, Pierce NA. Analytic adjoint solutions for the quasi-one-dimensional Euler equations. J Fluid Mech 2001;426:327–45.
[22] Arian E, Salas MD. Admitting the inadmissible: adjoint formulation for incomplete cost functionals in aerodynamic optimization. NASA/CR-97-206269, ICASE Report No. 97-69, 1997.
[23] Kim S, Alonso JJ, Jameson A. A gradient accuracy study for the adjoint-based Navier–Stokes design method, AIAA 99-0299. In: AIAA 37th aerospace sciences meeting and exhibit, Reno, NV, January 1999.
[24] Anderson WK, Newman JC, Whitfield DL, Nielsen EJ. Sensitivity analysis for Navier–Stokes equations on unstructured meshes using complex variables. AIAA J 1994;32(3):497–505.
[25] Taasan S, Kuruvila G, Salas MD. Aerodynamic design and optimization in one shot, AIAA 92-005. In: AIAA 30th aerospace sciences meeting and exhibit, January 1992.
[26] Jameson A, Kim S. Reduction of the adjoint gradient formula in the continuous limit, AIAA paper 2003-0040, AIAA 41st aerospace sciences meeting and exhibit, Reno, NV, January 2003.
[27] Kim HJ, Sasaki D, Obayashi S, Nakahashi K. Aerodynamic optimization of supersonic transport wing using unstructured adjoint method. AIAA J 2001;39(6).
[28] Mohammadi B, Pironneau O. Applied shape optimization for fluids. Oxford: Clarendon Press; 2001.
[29] Mohammadi B, Pironneau O. Shape optimization in fluid mechanics. Annu Rev Fluid Mech 2004;36:225–79.
[30] Denton JD. Loss mechanisms in turbomachines. ASME Paper 93-GT-435, 1993.
[31] Roe P. Approximate Riemann solvers, parameter vectors, and difference schemes. J Comput Phys 1981;43:357–71.
[32] van Albada GD, van Leer B, Roberts WW. A comparative study of computational methods in cosmic gas dynamics. Astron Astrophys 1982;108:76–84.
[33] Spalart PR, Allmaras SR. A one-equation turbulence model for aerodynamic flows. La Recherche Aerospatiale 1994:5–21.